fluids

MDPI

Review

Literature Review on Single and Twin-Screw Extruders Design for Polymerization Using CFD Simulation

Elham Delvar [1,2], Inês Oliveira [1,2], Margarida S. C. A. Brito [1,2,*], Cláudia G. Silva [1,2], Arantzazu Santamaria-Echart [3], Maria-Filomena Barreiro [3] and Ricardo J. Santos [1,2,*]

[1] Associate Laboratory in Chemical Engineering (ALiCE), Faculty of Engineering, University of Porto, 4200-465 Porto, Portugal; up202111358@edu.fe.up.pt (E.D.); up201906077@edu.fe.up.pt (I.O.); cgsilva@fe.up.pt (C.G.S.)

[2] Laboratory of Separation and Reaction Engineering—Laboratory of Catalysis and Materials (LSRE-LCM), Faculty of Engineering, University of Porto, 4200-465 Porto, Portugal

[3] CIMO, LA SusTEC, Instituto Politécnico de Bragança, Campus de Santa Apolónia, 5300-253 Bragança, Portugal; asantamaria@ipb.pt (A.S.-E.); barreiro@ipb.pt (M.-F.B.)

* Correspondence: mbrito@fe.up.pt (M.S.C.A.B.); rsantos@fe.up.pt (R.J.S.)

Abstract: This work presents a comprehensive review of the evolution in modeling reactive extrusion (REx), tracing developments from early analytical models to advanced computational fluid dynamics (CFD) simulations. Additionally, it highlights the key challenges and future directions in this field. Analytical models to describe the velocity profiles were proposed in the 1950s, involving certain geometrical simplifications. However, numerical models of melt polymeric flow in extruders have proven to be crucial for optimizing screw design and predicting process characteristics. The state-of-the-art CFD models for single and twin-screw extruders design address the impact of geometry (type of mixing elements and geometrical simplifications of CFD geometries), pressure and temperature gradients, and quantification of mixing. Despite the extensive work conducted, modeling reactive extrusion using CFD remains challenging due to the intricate interplay of mixing, heat transfer, chemical reactions, and non-Newtonian fluid behavior under high shear and temperature gradients. These challenges are further intensified by the presence of multiphase flows and the complexity of extruder geometries. Future advancements should enhance simulation accuracy, incorporate multiphase flow models, and utilize real-time sensor data for adaptive modeling approaches.

Keywords: reactive extrusion process; CFD simulation; polymerization; extruder designing

Academic Editors: Francesco De Vanna, Ernesto Benini and T. Hoehne

Received: 1 November 2024
Revised: 6 December 2024
Accepted: 28 December 2024
Published: 7 January 2025

Citation: Delvar, E.; Oliveira, I.; Brito, M.S.C.A.; Silva, C.G.; Santamaria-Echart, A.; Barreiro, M.-F.; Santos, R.J. Literature Review on Single and Twin-Screw Extruders Design for Polymerization Using CFD Simulation. *Fluids* **2025**, *10*, 9. https://doi.org/10.3390/fluids10010009

1. Introduction

Reactive extrusion is a fundamental process in polymer manufacturing where the material is forced to flow through a flow restriction, a die; a polymerization reaction takes place during the extrusion process. This process involves the polymerization, modification, or functionalization of polymers within the extruder. Reactive extrusion is widely used to modify the polymer molecular structure through crosslinking and grafting, to add reinforcements (fibers or fillers) to polymers during extrusion, or to promote the reaction between monomers to produce the final polymer. This technique is used to develop advanced materials, including high-performance composites, biodegradable plastics, and specialty polymers with enhanced chemical or mechanical properties.

The extruder consists of a hollow cylindrical barrel, where a screw is inserted and where the material is continuously dragged to the outlet through a die. Thus, the screw is

the most important component of an extruder and is divided into three main geometric zones: feeding, compressing, and mixing zones. These screw elements in the extruders facilitate fluid conveyance such as feeding, mixing, and compartmentalization of reactants into different zones [1,2]. The reactants must be homogenized, and the reactions must have enough time to complete before the process is complete. At the barrel's inlet, the reactants are fed into the extruder. In a standard extruder, the reactants are injected as a fluid or fed as solids in a hopper and at a specific stoichiometric ratio [3,4].

Over the years, Computational Fluid Dynamics (CFD) has emerged as a powerful tool for predicting and understanding the flow of polymer melting in extruders. It allows researchers to optimize their performance under different operating conditions without the need for expensive experimentation, saving material and energy costs. CFD simulations in REx facilitate the analysis of the complex interactions between fluid flow, heat transfer, and chemical reactions. The fluid flow affects the efficiency of mixing between reactants, and thus, CFD simulations enable the visualization of velocity fields, shear rates, and mixing patterns inside the extruder. These studies enable to optimize the screw design and geometry to enhance mixing and to ensure the uniform gradients of temperature and mass fraction of reactants. Since REx involves exothermic or endothermic reactions, the analysis of temperature gradients through CFD is crucial. CFD can predict the local overheating or underheating that can cause degradation and enable the identification of the best strategies to maintain a uniform temperature. Finally, CFD simulations enable the prediction of potential issues that arise during scale-up related to mixing or incomplete reaction and adjust process parameters accordingly.

REx usually involves the flow of polymer melting and the conveying of solids since pre-polymers or monomers in the solid state are fed to the extruder. Wilczyński, Nastaj [5] introduced a novel continuous concept for global modeling coupling, Discrete Element Modeling (DEM) for solid conveying and CFD modeling for molten polymer flow. This new approach solves the conservation equations as a continuum for the entire system without the need to segment the process into different zones (solid conveying, melting, and melt conveying). This enables a more precise prediction of extrusion behavior. Lewandowski and Wilczyński [6] reviewed the modeling approaches for the specific case of twin-screw extruders. Their work presents a comprehensive global model encompassing solid transport, polymer plasticating, and the flow of molten polymer. The authors highlight that advancements in these models are largely driven by the integration of DEM/CFD modeling techniques.

This paper presents a comprehensive literature review tracing the evolution from analytical expressions to CFD models predicting flow behavior in single and twin-screw extruders. The review is structured as follows: (i) an overview of extruder types, including single and twin-screw extruders; (ii) analytical models proposed in the literature to describe the flow in extruders using geometrical simplifications; (iii) a detailed review of CFD simulations, focusing on extruder geometries, mixing quantification, pressure and temperature gradients, and extruder design. Finally, the paper discusses the current challenges in implementing CFD models for REx and outlines future directions in this field.

1.1. Single-Screw Extruder

Single-screw extruders are characterized by just one screw located in the barrel. This equipment is easily manufactured, has a straightforward design, and is mechanically reliable. It uses frictional stress to promote the transport of solid materials, such as polymer pellets and particle fillers, and viscous stress to transport melt materials [7].

The single-screw extruder is widely used for simple applications, such as melting, plasticizing, and discharging melt for the manufacture of films, pipes, and profiles.

The schematic representation of the single-screw extruder is depicted in Figure 1. The major section of the extrusion system involves a screw which is rotating inside a barrel.

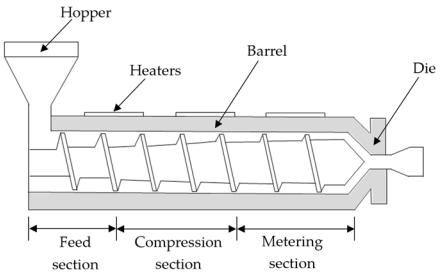

Figure 1. Schematic of components in Single-screw extruder.

1.2. TwinScrew Extruder

Twin-screw extruders are characterized by two screws located in the barrel. Twin-screw extruders are mainly used for processing heat-sensitive polymers, such as PVC, and in specialized applications like compounding, polymer filling, and reinforcement.

These devices can be categorized based on the screw rotation: a corotating extruder, when the screws turn in the same direction, counter-rotating extruder, when they rotate in opposite directions. Figure 2 shows a cross-section of two types of screws in the twin-screw extruders.

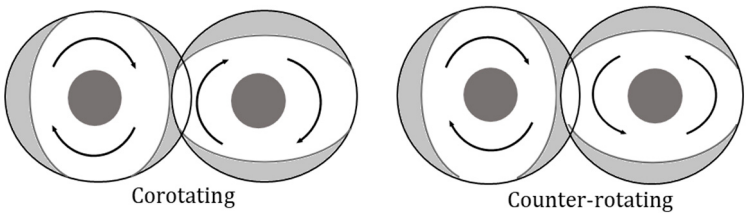

Figure 2. Cross section of corotating and counter-rotating extruder.

Furthermore, the distance between the screw shafts is also an important feature of screws. Non-intermeshing consists of tangential or separated screws, and intermeshing includes partial or full intermeshing, such as self-wiping screws. The screw configurations in co-rotating and counter-rotating extruders are shown in Figure 3.

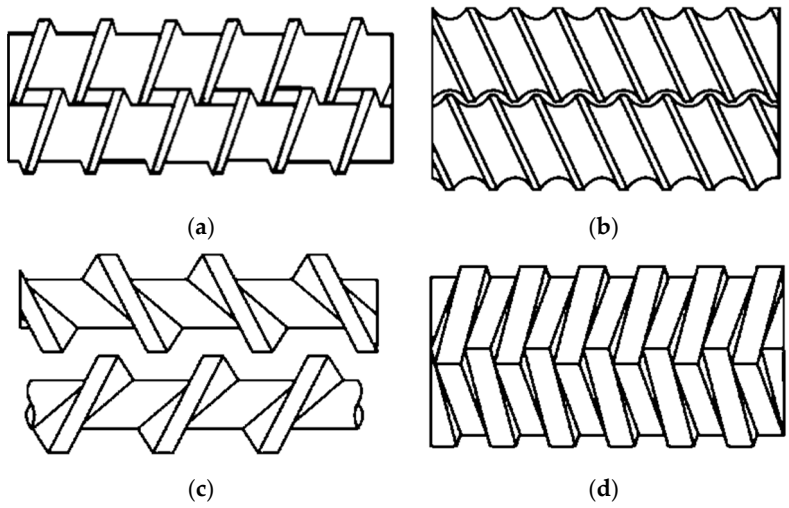

Figure 3. Intermeshing configuration for (**a**) partially intermeshing corotating, (**b**) closely intermeshing corotating, (**c**) tangential or non-intermeshing counter-rotating, and (**d**) closely intermeshing counter-rotating. Reprinted with permission from [8] (Permission reference 5899281196245).

Therefore, six types of twin-screw extruders can be used: tangential corotating, partially intermeshing corotating, closely intermeshing corotating, and the same types for counter-rotating extruders, respectively.

The applications of intermeshing corotating extruders depend on their speed. High-speed corotating extruders are used to add additives (colorants, fillers, reinforcements, stabilizers, etc.), devolatilization to remove solvents and reactive extrusion. Low-speed intermeshing corotating extruders are used to produce profiles and pipes. Non-intermeshing corotating extruders are not used in practice due to their poor mixing efficiency. Intermeshing counter-rotating extruders are used to compound PVC and other resin systems. Non-intermeshing counter-rotating extruders are efficient material conveyance and mixing, and therefore, they are used for devolatilization and chemical reactions.

1.3. Single-Screw Versus Twin-Screw Extruder

There are some differences between the processes occurring in single-screw and twin-screw extruders. The flow mechanism in twin-screw extruders differs significantly from those occurring in single-screw extruders. The complex flow patterns in twin-screw extruders enhance mixing and devolatilizing capabilities, heat transfer, and polymer melting efficiency. Moreover, the mixing mechanisms in twin-screw extruders are more efficient in intermeshing counter-rotating extruders and almost absent in non-intermeshing screws. Therefore, the twin-screw extruders are used in more complicated applications as homogenizers, dispersants of pigments and additives, reactive composition, concentration, evaporation, alloying, and polymerization [9].

On the other hand, in single-screw extrusion, the drag flow is predominant, and the transport efficiency is poor. This leads to poor mixing efficiency and a slow melting process.

Single and twin-screw extruders have different feeding processes. There are two types of feeding processes: gravity-fed (flood-feeding extrusion) or controlled by metering (starve-fed extrusion). Flood-feeding is typically used in single-screw extrusion where the feed hopper is filled, and the extruder screw rotation speed determines the feed rate. Starve feeding is typically used in twin-screw extrusion, where a feeder is used to meter the material into the system at a predetermined rate where rotation speed and throughput are independent of each other.

The implementation of twin-screw extruders for REx is more well established in the industry. Extensive control of residence time distribution and mixing and increased heat and mass transfer capability are the main reasons for this matter [10].

2. Analytical Models for Extruders

Both single and twin-screw extruders have complex geometries, making it difficult to analyze the flow in these devices. Analytical models have been proposed since the 1950s, introducing geometric conceptualizations that allowed for the derivation of analytical flow profiles. These models have been used as geometrical simplifications even for CFD models; therefore, it is crucial to present them here for better comprehension of the literature review on CFD for screw extruders.

2.1. Single-Screw Extruders

A base case for geometrical conceptualization is shown in Figure 4, which is the geometry of a typical metering section of a single-screw extruder. The main design parameters are the channel width, W, the flight width, e, the barrel diameter, D, the metering depth, H, the flight clearance, δ, and the helix angle, θ.

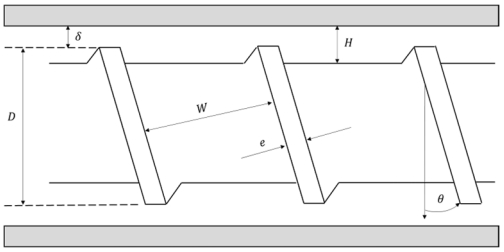

Figure 4. Geometry of a typical metering section of a single-screw extruder.

The melt flows within single-screw extruders were pioneered by Rowell and Finlayson [11] through an examination of flow dynamics in a "screw pump" for viscous oils. This analysis is based on drag and pressure flow concepts for an isothermal Newtonian fluid. Later, Maillefer [12] and Carley, Mallouk [13] applied this analysis to the extrusion of polymers, where the flow was analyzed by simplifying the screw geometry to a rectangular channel, which is known as the flat plate approximation. So, the screw should be visualized as uncoiled and laid flat, as it is represented in Figure 5, as well as the respective coordinate system.

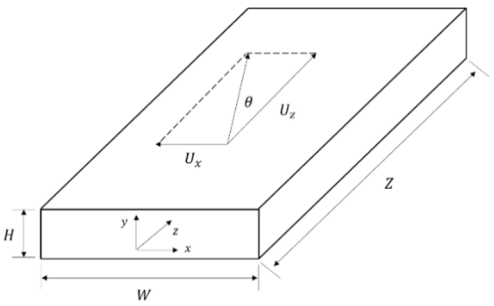

Figure 5. Unwound screw channel with the respective coordinate system.

If the channel's depth is significantly smaller than the outer diameter of the barrel, then the channel's curvature can be neglected. In this model, the side walls represent the leading and trailing surfaces of the screw flight, the upper surface corresponds to the screw root, and the bottom wall represents the inner surface of the barrel. The screw root moves across the channel at the screw's helix angle with a velocity $U = \pi DN$, where N is the screw rotational speed in rpm. The velocity U has two components of the screw's speed, U_x and U_z [14].

The formulation of the flows is based on several key assumptions: the flow is laminar and isothermal, the fluid is Newtonian and incompressible, and there is no slip at the walls [15]. The equations of motion, expressed in rectangular coordinates, assume that inertial terms are negligible in the steady state. Additionally, the equations are simplified using the lubrication approximation, meaning the velocities in the z-direction are fully developed and depend solely on the x and y coordinates. There is no y-component in the velocity terms, as its value is negligible for screws with a small channel depth-to-width ratio H/W. Therefore, the equations are given by:

$$0 = -\frac{\partial p}{\partial z} + \mu\left(\frac{\partial^2 u_z}{\partial x^2} + \frac{\partial^2 u_z}{\partial y^2}\right) \tag{1}$$

$$0 = -\frac{\partial p}{\partial x} + \mu\left(\frac{\partial^2 u_x}{\partial x^2} + \frac{\partial^2 u_x}{\partial y^2}\right) \tag{2}$$

The pressure gradient is constant and can be replaced by $\Delta p/Z$, where Δp is the pressure drop along the extruder and Z is the helical length. The dimension of the unwound

screw, Z, is related to the axial length of the metering zone of the extruder, L, through the following:

$$Z = \frac{L}{\sin(\theta)}$$

In Equation (1), the boundary conditions include $u_z = 0$ at the screw root and $u_z = -U\cos(\theta)$ on the barrel surface. Carley, Mallouk [13] solved the resultant flow between two parallel plates in relative motion, while omitting the effect of the screw flights. Equation (3) represents the integrated solution:

$$u_z = U_z \frac{y}{H} - \frac{1}{2\mu} y(H-y) \frac{\Delta p}{Z} \tag{3}$$

where $U_z = U\cos(\theta)$ and μ is the molecular viscosity. The velocity profile in Equation (3) involves two independent solutions. The first term, $U_z \frac{y}{H}$, also known as the drag flow, does not depend on the viscosity of the fluid and represents the maximum pumping capacity of the extruder. In the drag flow, the velocity changes linearly throughout the depth of the channel. The latter term, $\frac{1}{2\mu} y(H-y) \frac{\Delta p}{Z}$, commonly referred to as the pressure flow, depends on the viscosity and results in a parabolic distribution. The pressure flow only exists if the flow is restricted at the outlet through the presence of a die. Combining the drag and pressure flows yields the net velocity at each point. These velocity profiles are shown in Figure 6.

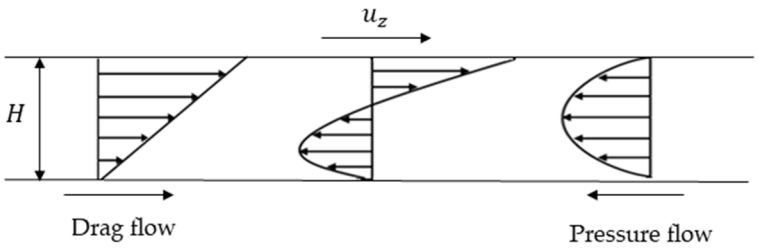

Figure 6. Velocity profiles in the parallel plane.

The axial component of the drag flow conveys the fluid forward along the channel while the pressure flow builds up in the reverse direction due to the resistance offered by the die at the outlet.

In addition to the discussed velocity profiles, there is also the transverse flow, analyzed, for the first time, by Mohr, Saxton [14] considering a Newtonian fluid. For Equation (2), the boundary conditions are $u_x = 0$ on the screw root and $u_x = -U\sin(\theta)$ on the barrel surface. Also, there can be no net flow of material in the x direction due to the sidewalls, i.e., the effect of the flight clearance, is omitted in this analysis. Therefore, $\int_0^H u_x dy = 0$, and the solution, which is known as the transverse flow, is represented as follows:

$$u_x = U_x \frac{y}{H} \left(2 - \frac{3y}{H}\right) \tag{4}$$

where $U_x = -U\sin(\theta)$. The respective velocity profile is shown in Figure 7.

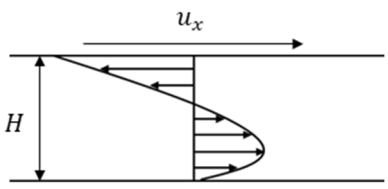

Figure 7. Velocity profile in the transverse plane.

The transverse flow moves the fluid toward the leading flight, after which the fluid is pushed downward to return to the bottom wall, creating a circulating motion that is very important for the mixing process within the extruder. As a result, the fluid element follows a helical path with an oval cross-section [14].

Concerning the discharge in the single-screw extruder, the outlet flowrate can be determined by integrating the product of u_z with the area of the screw channel from the top to the bottom, which results in $\int_0^H u_z W dy$ [13]. The outlet flow rate is given as follows:

$$Q = \frac{1}{2}\pi DHWNcos(\theta) - \frac{WH^3}{12Z}\frac{\Delta p}{\mu} \quad (5)$$

Equation (5) results from the difference between the flow rate for drag flow, $Q_D = \frac{1}{2}\pi DHWN\cos(\theta)$, and for the pressure flow, $Q_P = -\frac{WH^3}{12Z}\frac{\Delta p}{\mu}$. If there is no restriction, the extruder is in a state of "free discharge", or "open discharge", the pressure flow is zero and the flow rate at the outlet is given by $Q = Q_D$. If the equipment is closed off completely, there is no discharge, $Q = 0$, and the pressure build-up is maximum. This means that the drag flow is exactly offset by the pressure flow. As for the transverse component of the velocity, since it moves across the channel, it does not contribute to the output [16].

Furthermore, a leakage flow, Q_L, occurs in the clearance between the flight and the barrel due to the pressure difference created by the material being pushed forward by the screw. Therefore, the total flowrate of the extruder should be expressed as the difference between the flowrate for drag flow and the flowrates for pressure and leakage flows, $Q = Q_D - Q_P - Q_L$. However, since Q_L is usually much smaller than the other flow rates, it is often neglected when discharged by the extruder.

The power required by the extruder is also an important variable to consider. The power can be determined by the force's F work required to rotate the screw at a velocity U, resulting in $\dot{W} = FU$. The power is given as follows [17]

$$\dot{W} = \left(\frac{4\mu {U_x}^2}{H} + \frac{\mu {U_z}^2}{H} + \frac{U_z H}{2}\frac{\Delta p}{Z}\right) LW \quad (6)$$

Therefore, the basic performance variables that characterize the extruder are the outlet flowrate Q, the pressure buildup Δp and the power $\dot{W}$.

2.2. Twin-Screw Extruders

Studies regarding flow and geometry within the melt-conveying section of twin-screw extruders are scarce in the literature. The complexity of the flow also makes theoretical models for twin-screw extrusion less advanced compared to those for single-screw processes. The geometry and flows of the melt-conveying section of the two most common types of twin-screw extruders are analyzed here for self-wiping corotating (SWCOR) and closely intermeshing counter-rotating (CICTR).

2.2.1. Self-Wiping Corotating Twin-Screw Extruders (SWCORs)

Erdmenger [18] was one of the first to analyze its flow in the corotating extrusion field, concluding that material travels in the extruder according to the flow pattern disclosed in Figure 8. Also, it was demonstrated the close distance between screws enables them to clean each other surfaces of crust or layers of material caused by the pushing of material over to its mate. This improves the mixing efficiency and reduces the residues. Hence, the term "self-wiping" is used for this type of equipment.

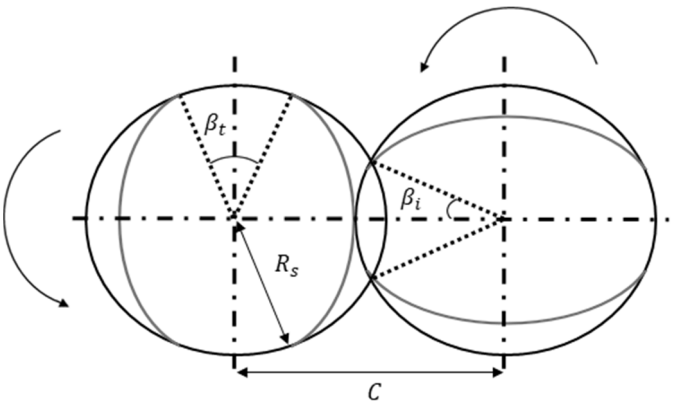

Figure 8. Cross section of a self-wiping intermeshing twin-screw extruder.

To gain further knowledge about melt-conveying flows in SWCORs, it is first necessary to describe their respective geometry. Booy [19] derived the cross-section geometry of a fully wiped corotating twin-screw extruder, which is represented in Figure 8, along with the centerline distance between two screws, C, screw radius, R_s, half the angle of intermeshing between two screws, β_i, and the tip angle of each screw, β_t.

Moreover, the cross-section of SWCORs presents a distinctive shape that is influenced by its diameter, centreline distance, and number of parallel channels or tips, n, due to the condition that one screw must wipe its counterpart, regardless of its position. This unique shape is determined by a kinematic analysis which provides equations that link design parameters and serve as the foundation for determining and selecting the screw dimensions. According to Figure 8, the centreline distance, C, screw radius, R_s, and intermesh angle, β_i, are related as follows:

$$C = 2R_s \cos \beta_i \tag{7}$$

Furthermore, β_i is related to β_t and n as follows:

$$\beta_i = \frac{\pi}{2n} - \frac{\beta_t}{2} \tag{8}$$

For the flow analysis, the channel cross-section geometry in a direction normal to the flights, which is shown schematically in Figure 9, must be considered. In Figure 9, it is represented the circumferential angle, φ, the channel's depth, H, and tip angle, β_t.

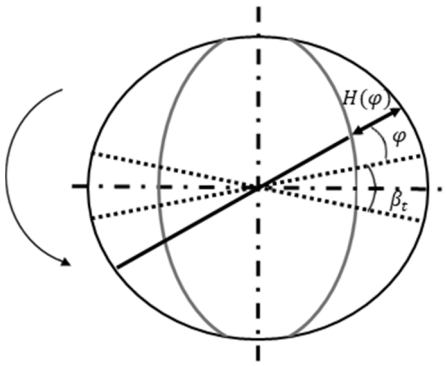

Figure 9. Channel's depth as function of the circumferential angle.

The channel's depth, H, is related to the circumferential angle, φ, through the following expression:

$$H(\varphi) = R_s(1 + \cos \varphi) - \sqrt{C^2 - {R_s}^2 \sin^2 \varphi} \tag{9}$$

The cross-channel depth profile can be plotted along the x axis, as it was represented for single-screw extruders. Figure 10 is a screw cross section in a plane perpendicular to the axis, representing both the x axis and channel's depth, $H(x)$.

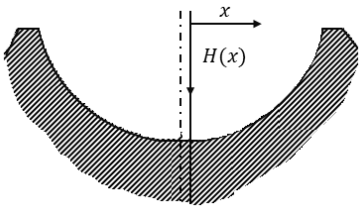

Figure 10. Screw cross-section plane perpendicular to the axis.

Denson and Hwang Jr. [20] modified Equation (9) to account for the helix angle and the flights' width, through the relation, $x = \frac{L\varphi\cos\theta}{2\pi} + \frac{e}{2}$. So, the expression for $H(x)$ is as follows:

$$H(x) = 2R_s - C \text{ for } 0 \le x \le \frac{e}{2} \tag{10}$$

$$H(x) = R_s\left[1 + \cos\left(\frac{2\pi\left(x - \frac{e}{2}\right)}{L\cos\theta}\right)\right] - \sqrt{C^2 - {R_s}^2\sin^2\left(\frac{2\pi\left(x - \frac{e}{2}\right)}{L\cos\theta}\right)} \text{ for } \frac{e}{2} \le x \le \frac{W}{2} \tag{11}$$

$$H(x) = 0 \text{ for } \frac{w}{2} \le x \le \frac{W + e}{2} \tag{12}$$

The open cross-sectional area between the barrel and the screw, A_p, proposed by Booy [19], is given by subtracting the cross-sectional area of the barrel, A_b, by the cross-sectional area of the two screws, $2A_s$, resulting in the following:

$$A_p = A_b - 2A_s \tag{13}$$

where,

$$A_b = 2(\pi - \beta_i){R_s}^2 + R_s C\sin\beta_i \tag{14}$$

$$A_s = n\left[\beta_i C^2 - CR_s\sin\beta_i\right] + \frac{1}{2}n\beta_t\left(C^2 + 2{R_s}^2 - 2CR_s\right) \tag{15}$$

$$A_p = 4{R_s}^2\left[\left(n - \frac{1}{2}\right)\beta_i + \left(n + \frac{1}{2}\right)\sin\beta_i\cos\beta_i - \pi\cos^2\beta_i + (\pi - 2n\beta_i)\cos\beta_i\right] \tag{16}$$

For the flows within screw elements in SWCORs, Denson and Hwang Jr. [20] examined an isothermal flow of incompressible Newtonian liquids for fully filled channels while neglecting the intermeshing region, which is valid when the flight tip angle, β_t, is small. Booy [21] and Szydlowski and White [22] extended this research by including the effects of the intermeshing region on the velocity field. White and Szydlowski [23] considered composite models of the flow rate and pressure profiles in modular twin-screw extruders involving both screw and kneading disks, which are mixing elements. Tayeb, Vergnes [24] developed a model based on solving thermal balance and Stokes equations in the melt-pumping section for an extruder with a deep screw channel.

This paper will discuss only the analysis, neglecting the intermeshing region [20]. As a simplification, similarly to the flat plate approximation of single-screw extruders, both the screw and barrel can be uncoiled. In this model, the barrel is treated as a flat plate moving with a velocity U, at an angle θ, relative to the stationary screw. However, for twin-screw extruders, the length of one unwound channel is the length of one turn of the screw. So, the model is a set of unwound channels alternating between each screw, as

represented in Figure 11. Moreover, the equations of motion and their respective boundary conditions are the same as for single-screw extruders, and therefore, the volumetric flow rate for each channel is the same as Equation (5). Consequently, to obtain the total flow rate, one must add the flow rates of all independent channels, given that there are $(2n-1)$ parallel channels [21].

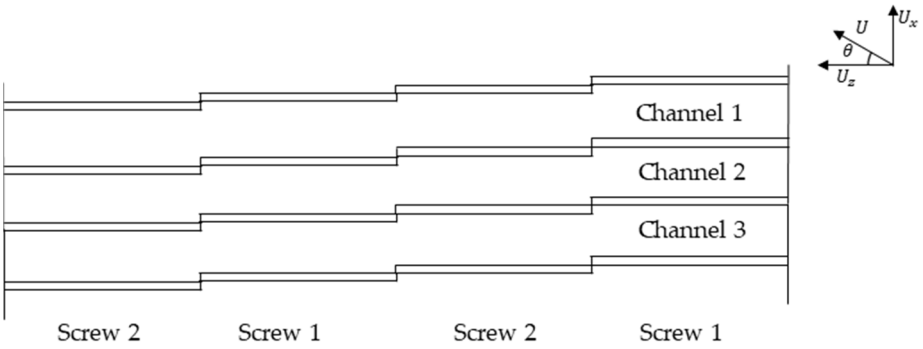

Figure 11. Unwound channels of screw elements.

Nevertheless, in most extrusion processes, screws are only partly filled with material, which is primarily related to the feeding scheme of the extruder since it is usually performed with metered feeding. Baird and Collias [25] demonstrated expressions for the calculation of velocity profiles and outlet flow rates depending on how much liquid is present within the extruder. The degree of fill of the channel is defined as the ratio of the filled channel cross-sectional area, A_f, to the total cross-sectional area, A, $f = \frac{A_f}{A}$. To obtain A, Equation (11) must be integrated across the width of the channel, which is given by

$$A = 4R_s^2\left[\frac{1}{2}\beta_i - \left(\beta_i + \frac{1}{2}\beta_t\right)\cos^2\beta_i + \left(\frac{1}{2}\sin\beta_i + \frac{1}{2}\beta_t\right)\cos\beta_i\right]\sin\theta \tag{17}$$

The velocity profiles in the z and x directions are as follows:

$$u_z = \frac{yU_z}{H} \tag{18}$$

$$u_x = \frac{3U_x y^2}{H^2} + \frac{4U_x y}{H} + U_x \tag{19}$$

To obtain the volumetric flow rate, Equation (18) should be integrated over the cross section that is filled with fluid, which results in the following:

$$Q = (2n-1)fA\pi R_s N\cos\theta \tag{20}$$

Note, from Equation (20), the flow rate is dependent on the degree of fill and screw parameters. On the other hand, the velocity profiles are independent of f, which implies that regardless of whether the screw channels are fully filled or partly filled with liquid, the axial velocity remains the same. This suggests that flow dynamics within the screw are primarily influenced by rotational speed and screw design and not by the volume of liquid present.

2.2.2. Closely Intermeshing Counter-Rotating Extruders (CICTR)

Kiesskalt [26] and Schenkel [27] denominated for the first time the intermeshing counter-rotating extruders as positive displacement pumps, with their flow rate determined by the screw geometry and screw speed. Kaplan and Tadmor [28] developed a theoretical model for flow in non-intermeshing twin-screw extruders under the assumption that this

equipment can result in a "three parallel plates" model, which leads to expressions for flow rate in terms of drag and pressure flow. Other works have analyzed the flow's mechanisms while considering the intermeshing level in the extruder [22,29].

The material transport in counter-rotating twin-screw extruders is made through a positive displacement mechanism, which is unique to this type of extrusion. Positive displacement depends on the degree of screw intermeshing, and it is most pronounced in CICTR. The flow takes place in a confined space known as the "C-shaped chamber", also known as the "C-chamber", where the maximum flowrate is as follows:

$$Q_{max} = 2nNV \tag{21}$$

where V is the volume of the C-chamber [25]. However, counter-rotating extruders may present leakage in certain regions of the screw and flights. Doboczky [30,31] and Janssen [32,33] analyzed the pumping characteristics of counter-rotating twin-screw extruders. Different types of flow in counter-rotating extruder are shown in Figure 12. Four key zones where leakage flow can occur were identified: flight flow (Q_f) through the gap between the flight and the barrel, calendaring flow (Q_c) between the bottom of the channel of one screw and the flight of the other screw, tetrahedron flow (Q_t) through the gap that goes from one screw to the other between the flanks of the flights of the two screws and side flow (Q_s) through the gap between the flanks of the screws perpendicular to the plane through the screw axis [32]. Moreover, Equation (20) can be corrected as follows:

$$Q = 2nNV - 2nQ_s - 2Q_f - Q_t \tag{22}$$

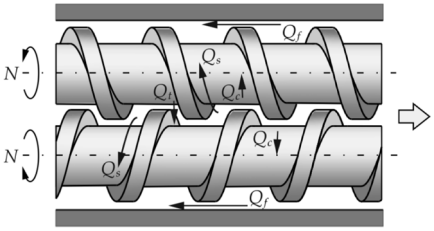

Figure 12. Types of flow in counter-rotating extruder, Q_f is leakage flow (screw flight and barrel), Q_c is calendaring flow (screw flight and opposite screw), Q_t is tetrahedron region, and Q_s is leakage flow (between the flanks of the screw). Reprinted permission from [34] (Permission reference 5898741218096).

3. CFD Simulation of Extruders

3.1. Single-Screw Extruders

Studies about single-screw extruders' computer modeling date back to the 1960s decade when Klein and Tadmor [35] assembled a mathematical model for the simulation of a plasticizing single-screw extruder, which was validated by experimental data. Additionally, Acur and Vlachopoulos [36] presented one of the first computer models for single-screw extruders, aiming at simulating the extrusion process of polymer while incorporating several components such as solids flow in the feed hopper and modified models for solids conveying and melting zone. Later on, Amellal, Lafleur [37] developed a model for a steady-state computer simulation of a single-screw extruder, which included the three zones of the extruder: solid-conveying, plasticizing, and metering section, which was crucial for the prediction of the extruder performance and to optimize its design and operating conditions. Then, Macgregor, Vlachopoulos [38] used a simulation methodology for conventional and barrier screws in order to predict the flow rate, pressure, and temperature profiles along the channel of the extruder.

These early works on extruder modeling paved the way for modern CFD models, which represent more sophistically complex three-dimensional flows and are going to be presented in the following sections.

3.1.1. Geometry

The geometry of single-screw extruders plays a major role in determining how material flows in the extruder and governs how they are transported, melted, and mixed. So, key geometric parameters, such as pitch, flight depth, and channel width and length, highly influence flow behavior and should be customized to meet the needs of the desired final product.

A literature review of the geometry used in the simulation of single-screw extruder is summarized in Table 1. As shown in Table 1, several geometries have been considered for single-screw extruders for CFD models. The flat plate model and helical geometries are geometrical simplifications, while simulations using z pin-type extruder, Dulmage-type screw, Saxton mixer, Faceted mixer, and Block-head mixer consider the actual geometry of the extruder.

Table 1. Summarized geometry of single-screw extruder used in literature.

Model	CFD Method	Geometry of CFD Model	Boundary Conditions	Research Focus
Flat plate model	FEM *	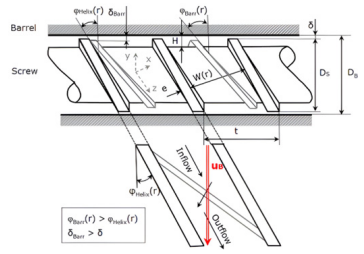 Reprinted with permission from Aigner, Köpplmayr [39]—Permission reference 5899410796913.	- Constriction of inlet mass flow rate. - Zero static pressure at the outlet. - Constant velocity at barrel surface.	Development of an approach to describe the flow behavior in barrier screws through CFD simulations in order to calculate the mass and pressure flow of different screw geometries.
	FDM **	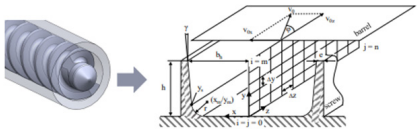 Reprinted with permission from Stueker and Schoeppner [40]—Permission reference 5899400520239.	- Stationary screw (bottom plate) ($u = 0$). - Moving barrel (top plate) with velocities of $U_x = -U\sin\theta$ and $u_z = U\cos\theta$. - Constant pressure gradient between inlet and outlet.	Analysis of the flow behavior of non-Newtonian polymer melts through the incorporation of real cross-sectional geometries of the screw channel.
	FEM	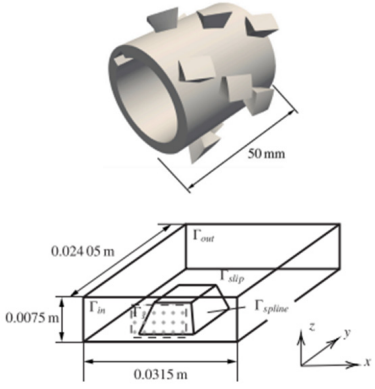 Reprinted with permission from Hube, Behr [41]—Permission references 5912470139350 and 5914101501361.	- Velocity of $U = \pi DN$ at the top plate (barrel surface). - Linear velocity profile, $u = \frac{U}{H}z$ at inflow. - Slip boundary conditions on both sides of the channel. - No-slip conditions on the bottom plate and mixing element. - Stress-free boundary conditions at the outflow. - Dirichet boundary conditions for the temperature on the top and bottom plates.	Introduction of a novel approach of shape optimization for the design of individual mixing elements with the help of the unwound mixing section to reduce computational complexity.

Table 1. *Cont.*

Model	CFD Method	Geometry of CFD Model	Boundary Conditions	Research Focus
Helical geometry and flat plate model	FVM ***	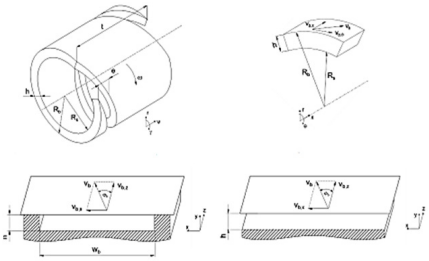 Reprinted with permission from Marschik and Roland [42]—Permission reference 5912460254971.	- Periodic boundary conditions between the inlet and outlet ($u_{in} = u_{out}$). - Velocities of the barrel of $U_x = U\sin\theta$ and $U_z = U\cos\theta$ for both models. - No-slip condition on the walls.	Comparison between flat plate model and curved screw channel through the prediction of the pumping capability of the extruder for a power-law fluid.
	FEM	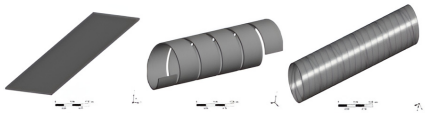 Reprinted from Ershov and Trufanova [43] (CC BY license).	- Moving screw with constant velocity defined at walls. - Constant temperature for body, screw, and input material.	Investigation of the effect of the shape of the channel and its effect on the flow mechanisms.
Helical geometry	FEM	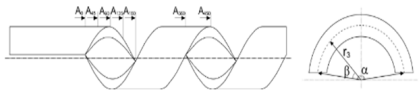 Reprinted from Kadyirov, Gataullin [44]. (CC BY license).	- Developed velocity profile at the inlet in the coaxial channel. - Fixed velocity of $U = -\pi DN$ at the tube wall. - No-slip conditions at the channel walls and surfaces of the screw shaft and flight.	Investigation of non-Newtonian solutions, specifically their effect on the flow structure and pressure drop.
	FEM	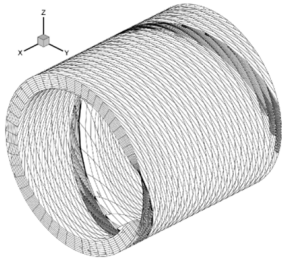 Reprinted with permission from Lim, Hwang [45]—Permission reference 5912441001952.	- Periodic boundary conditions between the inlet and outlet ($u_{in} = u_{out}$). - Stationary screw ($U = 0$). - Velocities of $u_x = 0$, $u_y = -U\sin\theta$ and $u_z = -U\cos\theta$ at the barrel wall. - Constant pressure gradient in the axial direction. - No-slip condition at the walls.	Introduction of a novel modeling technique to reduce simulation time and extruder's length by using a partial periodic unit of the geometry in the metering section.
	FEM	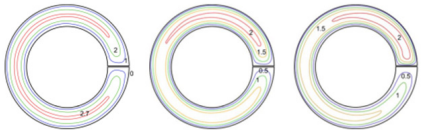 Reprinted from Vachagina, Kadyirov [46] (CC BY license).	- Developed velocity profile at channel inlet. - No-slip condition at the walls.	Modeling of a helical coordinate system to reduce the 3D problem to 2D for the study of melt flows through the helical geometry.
	FVM	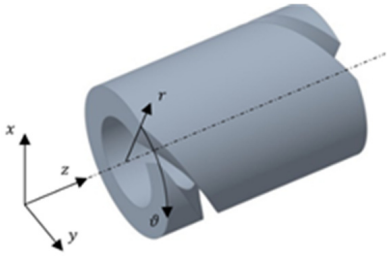 Reprinted from Herzog, Roland [47] (CC BY license).	- Periodic boundary conditions between the inlet and outlet ($u_{in} = u_{out}$). - Constant velocity at the barrel and zero velocity at the screw core. - Constant pressure gradient between inlet and outlet.	Introduction of a modeling method by including the 3D curved shape and the rotational motion of the screw channel boundaries.

Table 1. *Cont.*

Model	CFD Method	Geometry of CFD Model	Boundary Conditions	Research Focus
	FVM	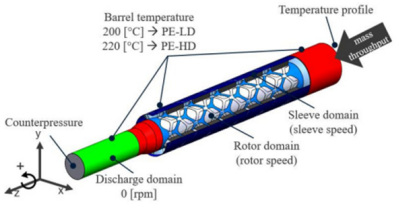 Reprinted from Janßen and Schiffers [48] (CC BY license).	- Mass throughput and temperature profile at the inlet. - Counterpressure at outlet. - Sleeve and rotor speed at sleeve and rotor domain, respectively. - Stationary discharge domain. - Constant barrel temperature.	Investigation of the influence of different materials on the performance of mixing sleeves and provide a new technique to predict the rotation speed of free-rotating mixers.
Pin-type extruder	FEM	 Reprinted with permission from Schöppner, Schadomsky [49]—Permission reference 5912460610087.	- Moving screw with speed adjusted to each simulation. - Constant barrel temperature. - Effects of wall sticking were not included.	Simulation of mixing behavior of rubber extruders through the investigation of new pin designs and geometries for process optimization.
Dulmage-type screw	FVM	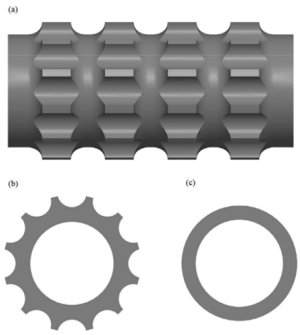 Reprinted with permission from Kimura, Nakayama [50]—Permission reference 5912460924947.	- Uniform axial velocity below the value for the flow rate at the inlet (from 10 kg/h and 30 kg/h). - Pressure of 0 Pa at outlet. - Zero velocity gradient in the normal direction. - Constant barrel surface temperature.	Investigation of mixing in a Dulmage-type screw to determine how it influences the operation conditions.
Saxton mixer	FVM	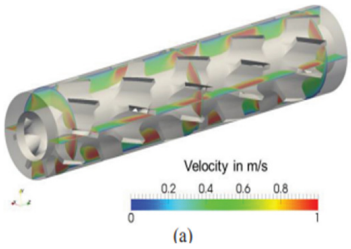 Reprinted with permission from Erb, Celik [51]—Permission reference 5912461232889.	- Moving screw with constant rotational speed.	Description of dispersive mixing through the calculation of the length stretch using an Eulerian frame and a Lagragian approach to apply in a 3D Saxton mixer.
Faceted mixer	*Not specified*	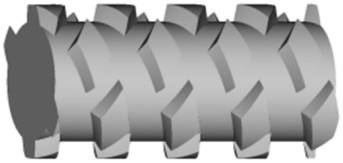 Reprinted with permission from Frank, Hollenhorst [52]—Permission reference 5912461412482.	- *Boundary conditions were not explicitly detailed.*	Design and optimization of the mixing geometry of a faceted mixer through CFD simulation for an examination of pressure throughput behavior for several designs.

Table 1. *Cont.*

Model	CFD Method	Geometry of CFD Model	Boundary Conditions	Research Focus
Pin barrel extruder	FEM	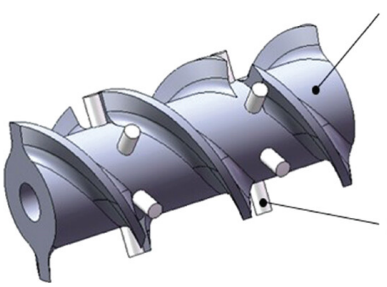 Reprinted from Wang, Pan [53] (CC BY license).	- Moving the screw with the rotational speed of *N*. - Calculated volume flow rate at the inlet, derived from the extrusion of output and material density. - Free flow at the outlet. - No-slip condition at the walls.	Proposal of a simple approximate mathematical model through the validation with simulation results for the quantitative assessment of elongational flow within extruders.
Block-head mixer	FEM	 Reprinted with permission from Marschik, Osswald [54]—Permission reference 5912470463105.	- Mass flowrate with a specific screw speed *N*. - Constant normal force with tangential velocities at the inlet. - Normal and tangential forces at the outlet. - No-slip condition at the walls.	Investigation of the pumping and mixing ability of a block-head mixer through the analysis of several geometrical parameters.

* FEM—Finite Element Method. ** FDM—Finite Difference Method. *** FVM—Finite Volume Method.

3.1.2. Quantification of Mixing

The mixing quality of the polymer in the melt-conveying section of single-screw extruders has significant effects on the properties of the final products. Over the years, several researchers have evaluated the mixing ability of single-screw extruders through CFD simulations to optimize mixing performance [51,55–58].

Two mixing concepts are distinguished in polymerization reactions: distributive and dispersive. Distributive mixing is related to the uniform distribution of fluids, and thus, the main mechanisms are stretching and folding. The efficient distributive mixing avoids the localized concentration gradients, ensuring a uniform reaction rate and consistent polymer properties. On the other hand, dispersive mixing is related to the reduction of particle/droplet size. The main mechanisms are related to the strong forces that promote the break of cohesive bonds. Distributive mixing is crucial for polymerization processes where fillers or reinforcement agents are introduced.

Several factors affect the "goodness" of mixing within the extruder. Frank and Schöppner [59] studied the balance between pressure consumption and mixing quality through CFD simulations. The goal was to develop a mixer combining a good relationship between these two parameters while using a faceted mixing section as a case study. Additionally, the effect of non-Newtonian polymers on flow patterns can influence the mixing performance on single-screw extruders and was recently investigated through the Lattice Boltzmann model, providing a reference frame to apply in the chemical industry [60].

CFD methods can be employed to evaluate the distributive and dispersive mixing quality, which is essential for achieving uniform melt and material homogenization [61–63]. Recently, Schulz, Vorjohann [64] optimized the distributive mixing in single-screw extruders by comparing two computational approaches for its prediction: the mean distance of streamlines and passive scalar integration, showing that the latter offers more advantages, particularly in its integration into the CFD environment and its better performance in longer mixing sections.

Kubik, Zatloukal [65] used as metrics for dispersive mixing quantification of the average stress criterion. This parameter is determined by the integral of stress (shear or elongational) along the chosen pathline over the residence time of the pathline. The analysis was performed using fluids with different rheological behaviors: the Carreau–Yasuda model and the White–Metzner model.

Residence time distribution (RTD) is a key measure for fluid non-homogeneities in extrusion. Moritzer, Wittke [66] developed a CFD model that predicts shear stresses and average residence times of materials within the extruder, enabling the accurate simulation of the internal conditions of the extruder and the prediction of extrusion performance. In addition, the RTD for the 3D circulatory flow expressed in terms of physical and geometrical parameters, such as flow rate, helix angle, aspect ratios, and many others, was presented by Kim [67], which is also very useful for understanding and predicting the RTD systematically through numerical analysis. Olofsson, Roland [68] introduced a CFD model designed for partially filled single-screw extruders for starve-feeding, which is a common industrial case. This work enables the characterization of the extruder fill length and RTD, paving the way for more accurate modeling and control of starve-feeding extrusion systems.

Additionally, Mateboer and Hummel [69] assessed distributive mixing using tracer particles and Shannon entropy calculations in CFD simulations, demonstrating that these methods effectively distinguish mixing quality across different extrusion simulations and identify the extruder that provides the most efficient mixing. Recently, Hopmann and Schön [70] addressed the importance of flow visualization of mixing processes by proposing an experimental setup while validating the findings through CFD simulations. This work made a significant contribution to the field of mixing examination of single-screw extruders, offering a novel setup capable of high spatial resolution, allowing for better distributive and dispersive mixing analysis.

CFD results of single-screw extruders combining chemical reactions and flow modeling are scarce in the literature. Nevertheless, the mixing characteristics of steady non-isothermal reactive flows in the metering section were investigated through the influence of some key parameters, concluding that while screw speed had minimal impact on flow efficiency, both the pressure-to-drag flow and channel aspect ratios significantly influenced the mixing [71]. Later, Roy and Lawal [72] performed an analysis using the flat plate model, investigating how several parameters such as power-law index, flowrate, and homogeneous and heterogeneous reaction parameters affect concentration profiles, axial conversion, and Sherwood number.

3.1.3. Modelling of Pressure and Temperature Gradients

Pressure and temperature profile studies provide insights for understanding extrusion processes. Moreover, some studies integrate the temperature and pressure distribution profiles since they directly influence how the material flows, the melting behavior, and the overall quality of the final product. CFD has been implemented to study the reference frame dependence of melt temperature rise in single-screw extruders, mainly whether it differs when the barrel rotates, and the screw is fixed and vice-versa [73]. This study incorporates a CFD model that enables the simulation of the 3D flow and temperature rise, concluding that the kinematics and the melt temperature rise are equal for either a rotating screw or a rotating barrel.

Other studies have included both pressure and temperature to provide a more complete knowledge of the flow's mechanisms [74,75]. For instance, Roland, Marschik [76] evaluated different data-based modeling approaches to predict the 3D non-linear throughput-pressure relationship of metering channels in single-screw extruders.

Abdel-Ghany and Ebeid [77] studied the screw performance at different operating temperatures and pressures by comparing two screw geometries: a traditional and a rapid compression one. Results showed that while pressure gradient has little effect on the screw's displacement, increasing temperature leads to an increase in displacement in both types of screws. Recently, Olofsson, Roland [68] also incorporated temperature and pressure gradients through the simulation of the flow and thermal behavior of a starve-feeding single-screw extruder, which helps to predict temperature distributions in both screw and barrel, providing a better understanding of how the material heats up and cools down during the process. It also addresses the pressure distribution by accounting for the partially filled nature of the extruder, predicting how the pressure builds up and varies along the length of the screw.

3.1.4. Validation of Extruder Throughput

The validation of expression (Equation (5)) that predicts the flow rate of a single-screw extruder is here described from a flat plate approximation. The validation was performed using a 3D CFD model using ANSYS/Fluent to solve the Navier–Stokes Equations, namely the continuity equation,

$$\nabla \cdot \mathbf{u} = 0 \tag{23}$$

and the momentum equation,

$$\rho\left(\frac{\partial \mathbf{u}}{\partial t} + \mathbf{u}\cdot\nabla\mathbf{u}\right) = -\nabla p + \mu\nabla^2\mathbf{u} \tag{24}$$

where $\mathbf{u}$ is the velocity vector, ρ and μ are density and viscosity, respectively, p is the pressure, and t is the flow time. The flow is isothermal in this work, so the energy equation was not solved. This set of equations neglects the body forces and considers an incompressible fluid, i.e., the density is constant.

Figure 13 shows the 3D CFD model of helical geometry and its respective coordinate system, where the dimensions used for the simulations were based on a single-flighted standard extruder (Fisher Scientific) with a diameter of D = 19 mm, a channel's width of W = 11.55 mm, a length of Z = 209.85 mm, a helix angle of θ = 14.11° and a flight clearance of δ = 0.5 mm [78].

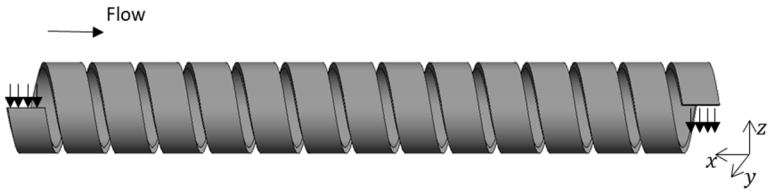

Figure 13. Spiral model of the single-screw extruder.

The flow was initially studied at a steady state. The method used for the pressure-velocity coupling was the coupled method. For the spatial discretization of gradient, pressure, and momentum, the Least Squares Cell Based, Second Order, and Second Order Upwind were used, respectively.

Regarding the initial solution for the steady state simulation, all flow variables were initialized with a value of zero, and 10^{-6} was set as a convergence criterion. The simulated fluid has a density of ρ = 1000 kg m^{-3} and a viscosity of μ = 0.1 Pa s.

The boundary conditions are the velocities imposed on the walls, which consist of one screw rotating within a barrel. The screw is moving at a rotational speed of N = 9.55 rpm. The tangential velocity at each position of the extruder wall was $U = \omega R_{screw}$, with the components U_x and U_z. Pressure conditions were defined at the inlet and at the outlet.

The validation of the CFD model was conducted by comparing the resulting outlet flowrate from the simulation to the one described earlier (Equation (5)); for the cases where the presence of a die is not simulated, $\phi = 0$, and is simulated, $\phi = -1/3$ and $\phi = -2/3$. Table 2. shows the theoretical results, along with the ones provided by CFD simulations, for the flow rate.

Table 2. Outlet flowrates for the different values of ϕ.

ϕ	Equation (5)/m^3 s^{-1}	CFD Simulation/m^3 s^{-1}
0	7.80×10^{-8}	7.99×10^{-8}
$-1/3$	5.20×10^{-8}	5.68×10^{-8}
$-2/3$	2.60×10^{-8}	3.61×10^{-8}

The results are, overall, in agreement with the ones proposed by the literature (Equation (5)). As it was expected, the outlet flow rate decreases as the pressure imposed at this surface increases, which results from the die configuration. However, deviations from the computed values of Equation (5) are more noticeable for higher pressure drops, which may be due to the conceptualization approaches of the model, resulting in inaccuracies in the results.

3.2. Twin-Screw Extruders

The complex design of twin-screw extruders, including intermeshing or non-intermeshing screws, screw profile, and barrel configuration, significantly influences flow dynamics, mixing efficiency, heat transfer, and pressure distribution. CFD models enable the optimization of screw design and process parameters, providing insights into performance enhancements for various polymer processing applications, from compounding to reactive extrusion.

3.2.1. Geometry

CFD simulations have been implemented to simulate the conveying zone (melting and mixing zone) and extrusion zone. A 3D modeling of the conveying zone is essential to capture detailed flow characteristics. Due to its complexity, simulations require fewer simplifications to the geometry. Table 3. shows a summarized research review on the geometry of twin-screw extruders.

Table 3. Summarized geometry of twin-screw extruder used in literature.

Rotation Screw Direction	CFD Method	Geometry of CFD Model	Boundary Conditions	Research Focus
Corotating screws	FEM	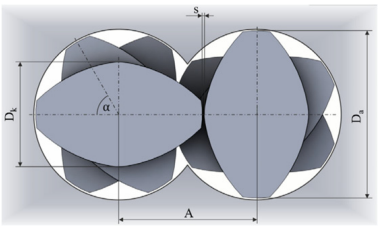 Reprinted with permission from Stritzinger, Roland [79] (Permission reference 5912480209160).	- Stationary barrel walls; - Zero velocity components at the barrel surface; - Velocity at the screw surface: $U = 2\pi Nr$; - Periodic boundary conditions between inlet and outlet.	Optimizing the extrusion process using a 3D model of a corotating intermeshing extruder with a kneading block for melt conveying to improve efficiency and power reduction.

Table 3. *Cont.*

Rotation Screw Direction	CFD Method	Geometry of CFD Model	Boundary Conditions	Research Focus
	FEM	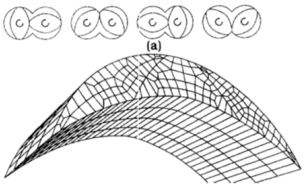 Reprinted with permission from Van Der Wal, Goffart [80] (Permission reference 5912490345777).	- Axial velocity is zero, $U_{screw} = 0$; - U_{barrel} is tangential according to the rotational speed; - No slip conditions at the barrel and screw surfaces; - Fully filled flow domain.	A 3D CFD model for a corotating extruder considers a simplification of the kneading block and studies the effect of parameters on mixing, such as shear rate and flow profile, by geometric simplification.
	SPH ****	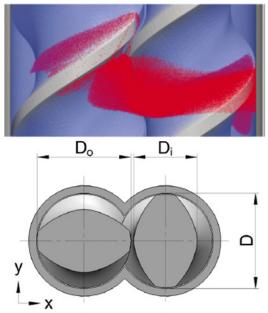 Reprinted with permission from [81,82] (Permission references 5912580169753 and 5912580479271).	- Periodic boundaries in the z-axis ($u_{in} = u_{out}$); - The screw speed was 95 rpm. - The barrel is stationary.	A SPH method considers a mechanistic model that takes into account the mass transfer along the screws and the heat transfer mechanisms.
	BEM *****	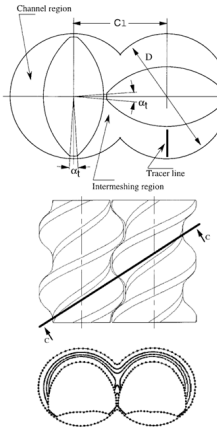 Reprinted from Rios, Gramann [83] (License CC BY).	- The geometry, a cut-long down-channel direction, remains fixed and moves in the axial direction as the screw rotates.	Self-wiping intermeshing corotating model is considered using BEM to study qualitative and quantitative mixing by various screw geometries, includingsingle, double, and triple flighted screws, by computing flow field, pressures, and stress. These simulations consider a flight clearance, a fully filled screw channel, and a Newtonian fluid.
	FEM	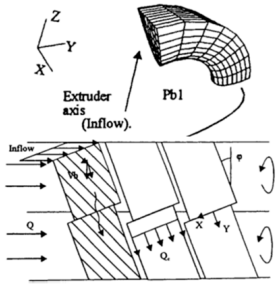 Reprinted with permission from Goffart, Van Der Wal [84] (Permission reference 5913010005059).	- The rotation speed is tangential to the barrel ($u_z = U\cos\theta$); - Inlet flow rate is imposed on the extruder; - The velocity of the screw is $U = 0$ m/s; - Free stress condition at the outlet plane.	A 2D CFD model of intermeshing corotating screws is used to analyze the flow profile, pressure build-up, and operational conditions. The fight clearance is neglected. The objective is to determine the throughput of the extruder by studying the effect of the rotation speed and the helix angle of the screw.

Table 3. *Cont.*

Rotation Screw Direction	CFD Method	Geometry of CFD Model	Boundary Conditions	Research Focus
	FEM	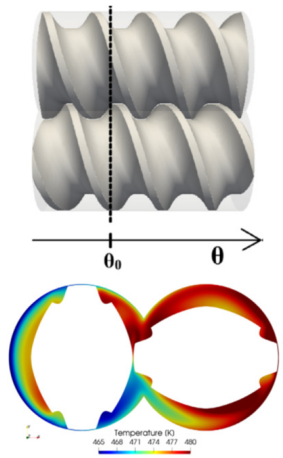 Reprinted with permission from Hinz, Helmig [85] (Permission reference 5913010808006).	- Screw speed 60,120 rpm; - No slip condition at the barrel; - Uniform inflow velocity was imposed at the inlet; - Inflow temperature $T_{inflow} = 473$ K.	Meshing techniques derived from the Snapping Reference Mesh Update Method (SRMUM) and Elliptic Grid Generation were used to simulate the flow in intermeshing corotating extruders using boundary-conforming meshes. The authors generated 2D spline-based geometries for selected screw orientations, which highlights the method's practicality for real-world applications. The density of the working flow is from 1 to 710 kg/m^3.
	FEM	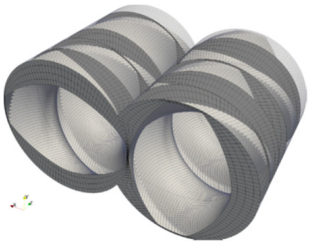 Reprinted with permission from Helmig, Behr [86] (Permission reference 5913030367101).	- No slip conditions at the barrel; - Dirichlet boundary condition of velocity on the rotating screw; - Inlet pressure is 0.2 MPa.	Authors used the boundary-conforming method to evaluate pressure and temperature distribution in two different screw configurations. The mesh update technique helps to compute the flow in the twin-screw extruder.
	FEM	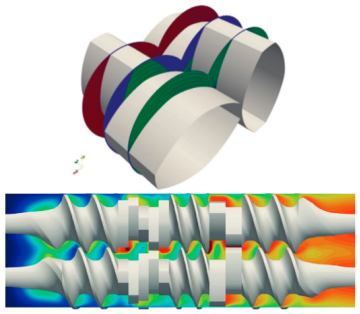 Reprinted with permission from Helmig, Key [87] (License CC BY).	- No slip condition at the barrel; - Atmospheric pressure at the outlet; - Temperature at inlet 473 K; - Adiabatic assumption for screws.	2D and 3D CFD simulation of Newtonian fluid requires the use of finely optimized boundary-conforming meshes within each subdomain, with coupling occurring only at the overlapping boundary interfaces.
	FEM	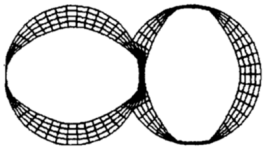 Reprinted with permission from Ishikawa, Kihara [88] (Permission reference 5913051404860).	- Constant flow rate at the inlet; - No slip at the barrel surface - Tangential velocity according to the screw speed for the disc surface; - Constant temperature at the inlet; - Adiabatic condition at disc surface.	A 3D CFD model investigates a simulation by using the FEM method for non-isothermal flow in the kneading disc area. Pressure gradient and temperature distributions at different rotational speeds were performed.

Table 3. *Cont.*

Rotation Screw Direction	CFD Method	Geometry of CFD Model	Boundary Conditions	Research Focus
	SPH	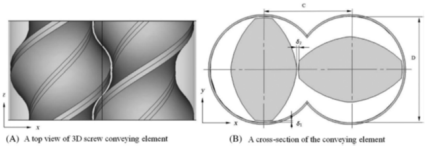 Reprinted with permission from Dong and Wu [89] (Permission reference 5913051404860).	- Periodic condition in z-direction ($u_{in} = u_{out}$); - No slip conditions at the barrel - Initial velocity of the fluid at screw set to zero.	3D CFD model of a conveying region using the SPH method for non-Newtonian fluid in fully and partially filled models. Two flight clearances were studied: 0 and 1 mm.
	SPH	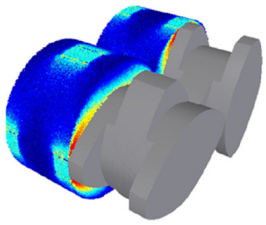 Reprinted with permission from Bauer, Matić [90] (Permission reference 5913100103435).	- No slip conditions at the barrel wall; - Velocity of the screw surface corresponds to rotational speed; - Periodic boundaries between inlet and outlet.	The CFD model evaluates the pressure build-up, power consumption, and mixing behavior of fully filled elements in different operational conditions. This model considers flight clearance.
Counter-rotating Screws	FEM	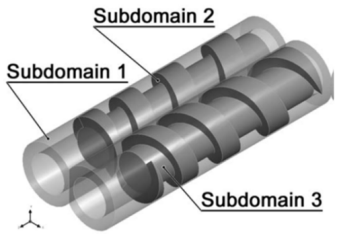 Reprinted with permission from Lewandowski, Wilczyński [91] (Permission reference 5912500224136).	- Flow rates imposed at the inlet were 4, 8, and 14 kg/h; - Screw speeds of 40 and 80 rpm; - Velocity is zero at the barrel wall.	The 3D model for a counter-rotating intermeshing region considers the screws simplification of the kneading block configuration.
	FEM	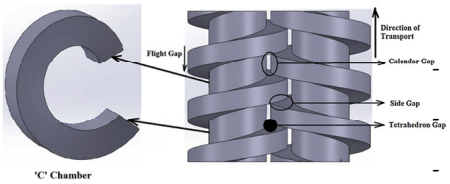 Reprinted with permission from S R, Arumugam [92] (Permission reference 5912970385230).	- Gravity effects were neglected; - Periodic boundary conditions ($u_{in} = u_{out}$); - No slip condition at the barrel wall.	A 3D CFD model using a 3D fully intermeshing counter-rotating extruder optimizes the production process with a minimum dissipation rate of viscosity and specific dimension of the final product. In this model, the Mesh Superposition Technique was used.
	FEM	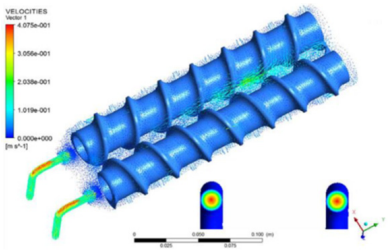 Reprinted from Yuan Zhang [93] (License CC BY).	- Inlet volume flow rate is $6.42 \times 10^{-5} m^3/min$; - Outlet is 6.25×10^6 Pa; - The screw rotational speed was 20 rotations/min.	A 3D model of non-intermeshing counter-rotating predicts a theoretical basis for the design and optimization of the die zone.

**** SPH—Smooth Particle Hydrodynamics. ***** BEM—Boundary Element Method.

3.2.2. Quantification of Mixing

A comprehensive state-of-the-art mixing analysis using CFD simulation is presented here for twin-screw extruders [94–102]. Starting with the state-of-the-art implementation of residence time distribution (RTD) in twin-screw extruders, Bauer and Matić [101] studied

the local RTDS in specific regions of the twin-screw extruders. The measurement of local RTDs is a limitation of experiments that only measure the total RTDs in the extruder. The impact of variations in screw speed, throughput, and screw length in local RTDs from-tracer experiments using the SPH method. The CFD simulations helped to understand the impact of the residence time on mixing and predict quantitative mixing per screw revolution. These results were validated from tracer experiments. Robinson and Cleary [103] simulated RTD in twin-screw extruders for particle filling factors (50%) using a Lagrangian method that enabled the tracking of particle positions. Over time, the mixing process improves due to the theoretically infinite residence time resulting from the use of a periodic domain in the axial direction. Mixing efficiency was assessed using the Finite-Time Lyapunov Exponent (FTLE) method and another approach based on the homogeneity of initial color distributions. This approach enabled the quantitative mixing separately in both the cross-sectional and axial directions of the chamber, providing a comprehensive analysis of the process.

Oldemeier and Schöppner [104] investigated the mixing performance of five various configurations of screw elements in a corotating extruder through 3D CFD flow simulations. They combined CFD simulation with particle tracking techniques to achieve both dispersive and distributive mixing, optimizing the extruder mixing section. To obtain distributive mixing, the spatial distribution of particles was evaluated, and a mixing index was determined. To obtain dispersive mixing, the maximum shear stress along the particle paths and the integral of shear stress for each particle's residence time were calculated. They concluded that screw geometry and rotational speed significantly affect both types of mixing.

Alsteens, Legat [99] evaluated the mixing efficiency from the comparison between the residence time and the shear distribution, which are commonly used as metrics for mixing quantification. A set of particles was introduced to the system in kneading blocks. In this study, the stagger angles and number of discs are studied.

Eitzlmayr and Khinast [81] first quantified mixing from the time evolution of the intensity of segregation using the tracer particles for the partially and totally filled regions using the SPH model. On the other hand, the mixing was evaluated using the fitted kinetic laws to determine the mixing rates. This analysis was made separately to analyze the overall mixing and axial mixing and to conclude the axial and cross mixing to the overall mixing rate. Eitzlmayr, Matić [82] evaluated the mixing using the SPH method for different geometries of corotating twin-screw elements, two kneading elements and a mixing element. The mixing analysis was performed based on the time-dependent evolution of the intensity of segregation related to various tracers. The exponential mixing rates describe the decrease in the intensity of segregation per screw revolution. Kwag and Lyu [105] also quantified mixing from the reaction kinetics. The production of polypropylene through a 3D CFD simulation was studied using a corotating extruder using ANSYS Polyflow. The study examined the impact of factors such as screw rotation speed, kneading block stagger angle, and inlet flow rate influenced the mixing and reaction processes. The findings demonstrated that these operational and geometric parameters significantly impact mixing efficiency, residence time distribution, flow temperature, local species concentration, reaction time and rate, and overall conversion rate.

Sarhangi Fard and Anderson [106] implemented a mapping method to analyze and quantify mixing in kneading blocks in a twin-screw extruder. They studied different staggering angles for the kneading blocks. Also, the mixing efficiency of the screw mixing elements was compared with the standard elements of conveying zone. The results demonstrated that the stagger angle has a significantly greater influence on distributive mixing compared to the width of the screw disc.

The impact of different filling factors on both distributive and dispersive mixing characteristics in counter-rotating extruder was evaluated by Ahmed, Poudyal [107]. Although the simulations were conducted in 2D, valuable insights were gained regarding the influence of the filling factor on mixing. The dispersive and distributive mixing were assessed using the mixing index, cumulative distribution of maximum shear stress, cluster distribution index, scale of segregation, and length of stretch calculated from massless particles. Results show that filling factors between 70% and 80% present the best results in terms of distributive and dispersive mixing.

3.2.3. Modelling of Pressure and Temperature Gradients

Temperature and pressure gradients in twin-screw extruders have been simulated using CFD simulations to reach the desired viscosity and homogeneity, facilitating the mixing efficiency and preventing degradation or incomplete melting. The effect of viscosity and velocity on thermal distribution and flow behavior was studied by Ahmed, Poudyal [107]. They concluded that by increasing time, shear results and velocity values rose. This causes an increase in temperature gradient.

Sun, Zhu [108] performed a 3D numerical simulation of a corotating twin-screw extruder to analyze the impact of the screw's rotational speed on the temperature gradient. Results show that the increase in screw rotational speed enhances the increase in temperature. This occurs because a higher rotational speed generates a larger shear rate and, thus, viscous dissipation. However, while the larger pressure drop can speed up material flow, it reduces the residence time of materials, which can negatively impact the efficiency of mixing and polymerization reactions along the axial direction.

Bertrand, Thibault [109] employed a 2D simulation of fluid flow in corotating twin-screw and performed the pressure profiles plotting pressure versus the location of the screws at two different temperatures. The authors showed that when the position of the screw tip is away from the barrel, the pressure value decreases. Moreover, when the position of the screw tip is close to the peak of the nip region of two screws, the pressure increases.

Lewandowski, Wilczyński [91] analyzed the pressure and temperature gradients for a non-Newtonian fluid at different flow rates and screw speeds using 3D simulations in a closely intermeshing counter-rotating extruder. The results showed that the pressure can be increased or decreased in different parts of the screw. At the C-chamber region, pressure decreases and increases at the gap between the flights.

Eitzlmayr and Khinast [110] explore the pressure gradients in Newtonian, isothermal flows within a twin-screw extruder. The pressure gradients (0–35 kPa/m) were validated using the SPH method and shown to scale proportionally with viscosity in creeping flow. However, this simulation assumed isothermal conditions, i.e., the temperature gradients were not considered, limiting the application to real processes. The authors point out that future works must incorporate non-isothermal effects, as neglecting local energy distribution and temperature inhomogeneities could introduce significant errors.

Martelli [111] studied the temperature and pressure gradients in the melt section by considering Newtonian flow in the non-intermeshing counter-rotating extruder. They illustrated two major issues in the conveying zone: the first is how material distribution across different processing zones can be controlled through the use of reverse screw elements, and the second is generating backpressure by these elements.

Nakayama, Takemitsu [112] developed a method to improve mixing characteristics by playing with the pressure gradients using 3D CFD simulation of fully filled, non-isothermal molten polymer in the mixing section. They studied the effect of geometry with both forward and backward configurations of pitched tips of the kneading block on mixing efficiency. Results showed that the geometry of the mixing elements affects the flow's

direction and pressure at a certain rotational speed and flow rate throughout the channel. They concluded that the pumping ability was obtained by the disk-stagger angle and tip angle. A positive or a negative amount of the pressure gradient shows that the pressure flow happens on the average of the forward or backward direction of the channel.

Die configuration and the number of dies at the outlet have significant effects on pressure distribution. Yuan Zhang [93] concluded, from CFD simulations, that the pressure gradient by adding two and three dies at the end of a twin-screw extruder. The maximum pressure is in both cases, but the pressure first decreased from the entrance to the die and then increased.

4. Challenges of CFD Models of Reactive Extrusion

This review highlights fundamental studies of mixing mechanisms and flow dynamics in reactive extrusion (REx) using screw extruders, dating back to the 1950s when analytical models were first proposed. These early models provided critical insights and have since been used to simplify geometries in CFD simulations. CFD simulations have been extensively utilized to investigate the effects of various screw element shapes and operating conditions, such as rotation speed and direction, on mixing performance. These studies quantify mixing efficiency using metrics, such as residence time distributions (RTDs) and flow deformation, while also examining the influence of pressure and temperature gradients on mixing efficiency and outlet flow rates. However, REx flows remain highly complex, and accurately simulating the full geometry of extruders is essential for successfully implementing these units in industrial applications.

Modeling reactive extrusion using CFD faces significant challenges due to the intricate interplay of physical and chemical processes. REx involves mixing, heat transfer, and chemical reactions within non-Newtonian fluids subjected to high shear forces and temperature gradients. Capturing these phenomena requires advanced rheological models to account for the material's non-Newtonian behavior and robust kinetic models to describe chemical transformations. Multiphase flows, such as gas generation and particle formation, add further layers of complexity. Additionally, extruder geometries, especially the flight clearance between the screw and barrel, demand high-resolution meshes, making simulations computationally intensive. Finally, validation of these models is also constrained by the limited availability of in situ measurements and the challenges of replicating industrial conditions at a laboratory scale.

Future research should aim to improve the accuracy and efficiency of CFD simulations to better capture complex phenomena such as mixing, heat transfer, and chemical reactions. Addressing multiphase flow modeling, including gas generation and particle interactions, is critical; it can be performed using a global model that combines DEM/CFD simulations, as proposed by Wilczyński, Nastaj [5]. Moreover, incorporating real-time sensor data during extrusion processes could enable dynamic and adaptive modeling, paving the way for more reliable industrial applications.

5. Conclusions

CFD models have been intensively explored for REx, offering valuable insights for industrial applications. These CFD models have evolved from mere geometric conceptualizations of extruders to actual geometric simulations. This work presents a literature review on single and twin-screw extruders, primarily focusing on the geometries of CFD models, studies on reactive mixing, and modeling of pressure and temperature gradients. The influence of geometrical configurations (e.g., mixing element shapes) and operating conditions (such as rotation speed, relative screw direction in twin extruders, and pressure and temperature gradients) has been extensively investigated. Additionally, the analytical

expression that describes the outlet flow rate was validated here using CFD simulations of a helical geometry to calculate the outlet flow rate. However, the results reveal discrepancies between the model, which assumes simplified flow conditions, and the CFD results, particularly due to flow restrictions at the outlet caused by the presence of a die.

While numerous studies have explored various geometries and flow constrictions in reactive extrusion using CFD, significant challenges remain due to the complex interactions between physical and chemical processes. REx involves mixing, heat transfer, and chemical reactions in non-Newtonian fluids under high shear and temperature gradients, requiring detailed rheological and kinetic models. The presence of multiphase flows, such as gas generation and particle formation, further complicates simulations. Additionally, the extruder's geometry, particularly flight clearance, necessitates high-resolution meshes, increasing computational demands. Validation is also hindered by limited access to in situ data and challenges in replicating industrial conditions at the lab scale. Future efforts should improve simulation accuracy and efficiency, address multiphase flow modeling, and incorporate real-time sensor data to enable more dynamic and adaptive modeling approaches.

Author Contributions: Conceptualization, E.D., I.O., M.-F.B., A.S.-E., C.G.S., R.J.S. and M.S.C.A.B.; methodology and formal analysis, E.D., I.O. and M.S.C.A.B.; writing—original draft preparation, E.D., I.O. and M.S.C.A.B.; writing—review and editing, R.J.S., C.G.S. and M.S.C.A.B.; supervision, M.-F.B., A.S.-E., C.G.S., M.S.C.A.B. and R.J.S.; project administration, M.-F.B., C.G.S., R.J.S., All authors have read and agreed to the published version of the manuscript.

Funding: This work was supported by BioShoes4All (PRR–000011), supported by PRR—Plano de Recuperação e Resiliência—Bioeconomia. This research was also supported by national funds through FCT/MCTES (PIDDAC): LSRE-LCM-UIDB/50020/2020 (DOI: 10.54499/UIDB/50020/2020) and UIDP/50020/2020 (DOI: 10.54499/UIDP/50020/2020); and ALiCE—LA/P/0045/2020 (DOI: 10.54499/LA/P/0045/2020), CIMO UIDB/00690/2020 (DOI:10.54499/UIDB/00690/2020) and UIDP/00690/2020 (DOI:10.54499/UIDP/00690/2020); SusTEC LA/P/0007/2020 (DOI:10.54499/LA/P/0007/2020). Elham Delvar acknowledges her PhD scholarship supported by Fundação para a Ciência e Tecnologia (FCT) (2023.01245.BD). Margarida S.C.A. Brito acknowledges her contract (2023.06416.CEECIND) supported by the FCT Individual Call to Scientific Employment Stimulus—6th Edition.

Conflicts of Interest: The authors declare no conflict of interest.

List of Variables

A	channel's cross-sectional area [m^2]
A_b	barrel's area [m^2]
A_f	filled channel's cross-sectional area [m^2]
A_p	area between the barrel and the screw [m^2]
A_s	screw's area [m^2]
C	centerline distance [m]
D	diameter of the extruder [m]
e	flight's width [m]
F	force's work [N]
f	degree of fill
H	channel's height [m]
N	screw velocity [rpm]
n	number of tips
p	pressure [Pa]

Q	flowrate [$m^3\ s^{-1}$]
Q_{max}	maximum flowrate [$m^3\ s^{-1}$]
Q_c	calendaring flowrate [$m^3\ s^{-1}$]
Q_f	flight flowrate [$m^3\ s^{-1}$]
Q_s	side flowrate [$m^3\ s^{-1}$]
Q_t	tetrahedron flowrate [$m^3\ s^{-1}$]
$R_{clearance}$	distance between the rotation axis and the flight's clearance surface [m]
R_{screw}	distance between the rotation axis and the screw surface [m]
R_s	screw's radius [m]
t	time [s]
U	velocity [$m\ s^{-1}$]
u	velocity profile [$m\ s^{-1}$]
$\mathbf{u}$	velocity vector field [$m\ s^{-1}$]
U_x	velocity in the x component [$m\ s^{-1}$]
u_x	velocity profile in the x component [$m\ s^{-1}$]
U_x	velocity in the z component [$m\ s^{-1}$]
u_z	velocity profile in the z component [$m\ s^{-1}$]
W	channel's width [m]
$\dot{W}$	power consumption [m]
x	space coordinate [m]
y	space coordinate [m]
Z	helical length [m]
z	space coordinate [m]
Greek letters	
α_i	volume fraction of species i
β_i	intermesh angle [°]
β_t	tip angle [°]
δ	flight's clearance [m]
θ	helix's angle [°]
μ	dynamic viscosity [Pa s]
ρ	density [$kg\ m^{-3}$]
φ	circumferential angle [°]
ω	angular velocity [$rad\ s^{-1}$]
ϕ	pressure-to-drag flow ratio
VIC	variable intermeshing clearance

References

1. Scott, H.G.; Humphries, J.F. Modern Pelastic. Patent WO2004009356A1, March 1973.
2. Hopmann, C.; Adamy, M.; Cohnen, A. *Introduction to Reactive Extrusion: Principles and Applications*; Wiley-VCH Verlag GmbH & Co. KGaA: Hoboken, NJ, USA, 2017; pp. 1–10.
3. Biermann, L.; Brepohl, E.; Eichert, C.; Paschetag, M.; Watts, M.; Scholl, S. Development of a continuous PET depolymerization process as a basis for a back-to-monomer recycling method. *Green Process. Synth.* **2021**, *10*, 361–373. [CrossRef]
4. Misiura, D.; Majka, T.M. An overview on obtaining foamed PET by reactive extrusion. *Tech. Trans.* **2018**, *115*, 97–102.
5. Wilczyński, K.; Nastaj, A.; Lewandowski, A.; Wilczyński, K.J.; Buziak, K. Fundamentals of Global Modeling for Polymer Extrusion. *Polymers* **2019**, *11*, 2106. [CrossRef]
6. Lewandowski, A.; Wilczyński, K. Modeling of Twin Screw Extrusion of Polymeric Materials. *Polymers* **2022**, *14*, 274. [CrossRef] [PubMed]
7. Cassagnau, P.; Bounor-Legaré, V.; Fenouillot, F. Reactive Processing of Thermoplastic Polymers: A Review of the Fundamental Aspects. *Int. Polym. Process.* **2007**, *22*, 218–258. [CrossRef]
8. Martin, C. Twin Screw Extruders as Continuous Mixers for Thermal Processing: A Technical and Historical Perspective. *AAPS Pharmscitech* **2016**, *17*, 3–19. [CrossRef]
9. Tsao, T.F.; Harper, J.M.; Repholz, K.M. The effects of screw geometry on extruder operational characteristics. *AlChE Symp* **1978**, *74*, 142–147.

10. Kousemaker, T.M.; Druetta, P.; Picchioni, F.; Vakis, A.I. Modelling supercritical CO_2 flow in a co-rotating twin screw extruder using the level-set method. *Chem. Eng. Res. Des.* **2024**, *205*, 569–577. [CrossRef]
11. Rowell, H.; Finlayson, D. Screw viscosity pumps. *Engineering* **1928**, *126*, 639.
12. Maillefer, C. Etude théorique et expérimentale sur le fonctionnement des boudineuses. Doctoral thesis, Available online, 1952. Available online: https://infoscience.epfl.ch/entities/publication/50539f50-40fd-4810-b473-37fceb10d636 (accessed on 1 November 2024).
13. Carley, J.F.; Mallouk, R.S.; McKelvey, J.M. Simplified Flow Theory for Screw Extruders. *Ind. Eng. Chem.* **1953**, *45*, 974–978. [CrossRef]
14. Mohr, W.D.; Saxton, R.L.; Jepson, C.H. Theory of Mixing in the Single-Screw Extruder. *Ind. Eng. Chem.* **1957**, *49*, 1857–1862. [CrossRef]
15. Li, Y.; Hsieh, F. Modeling of flow in a single screw extruder. *J. Food Eng.* **1996**, *27*, 353–375. [CrossRef]
16. Carley, J.F.; Strub, R.A. Basic Concepts of Extrusion. *Ind. Eng. Chem.* **1953**, *45*, 970–973. [CrossRef]
17. Middleman, S. Extrusion. In *Fundamentals of Polymer Processing*; McGraw-Hill College: New York, NY, USA, 1997; pp. 123–169.
18. Erdmenger, R. Mehrwellen-Schnecken in der Verfahrenstechnik. *Chem. Ing. Tech.* **1964**, *36*, 175–185. [CrossRef]
19. Booy, M.L. Geometry of fully wiped twin-screw equipment. *Polym. Eng. Sci.* **1978**, *18*, 973–984. [CrossRef]
20. Denson, C.D.; Hwang, B.K. The influence of the axial pressure gradient on flow rate for Newtonian liquids in a self wiping, co-rotating twin screw extruder. *Polym. Eng. Sci.* **1980**, *20*, 965–971. [CrossRef]
21. Booy, M.L. Isothermal flow of viscous liquids in corotating twin screw devices. *Polym. Eng. Sci.* **1980**, *20*, 1220–1228. [CrossRef]
22. Szydlowski, W.; White, J.L. An improved theory of metering in an intermeshing corotating twin-screw extruder. *Adv. Polym. Technol.* **1987**, *7*, 177–183. [CrossRef]
23. White, J.L.; Szydlowski, W. Composite models of modular intermeshing corotating and tangential counter-rotating twin screw extruders. *Adv. Polym. Technol.* **1987**, *7*, 419–426. [CrossRef]
24. Tayeb, J.; Vergnes, B.; Valle, G.D. A Basic Model for a Twin-Screw Extruder. *J. Food Sci.* **1989**, *54*, 1047–1056. [CrossRef]
25. Baird, D.G.; Collias, D.I. Extruders. In *Polymer Processing*; Brenner, H., Ed.; Butterworth-Heinemann: Oxford, UK, 1995; pp. 235–240.
26. Kiesskalt, S. Untersuchungen an einer Kapsel Pumpe. *VDI Zeitschr* **1927**, *71*, 453.
27. Schenkel, G. *Kunststoff-Extrudertechnik: Konstruktionsgrundlagen und Betriebstechnik der Kunststoff-Schneckenpressen*; Carl Hanser Verlag: Munich, Germany, 1963.
28. Kaplan, A.; Tadmor, Z. Theoretical model for non-intermeshing twin screw extruders. *Polym. Eng. Sci.* **1974**, *14*, 58–66. [CrossRef]
29. Kim, M.H.; Szydlowski, W.; White, J.L.; Min, K. A new model of flow in a tangential counter-rotating twin screw extruder. *Adv. Polym. Technol.* **1989**, *9*, 87–95. [CrossRef]
30. Doboczky, Z.E. Doppelschnecke. *Plastverarbeiter* **1965**, *16*, 57–67.
31. Doboczky, Z. Theoretische and wirkliche Ausstoßleistung der Doppelschnecken Extruder. *Plastverarbeiter* **1965**, *16*, 395–400.
32. Janssen, L. *Twin Screw Extrusion*; Elseviers Sci. Publ. Company: Amsterdam, The Netherlands, 1978.
33. Janssen, L.P.B.; Lphrm, M.; Jm, S. A Model for the Output from the Pump Zone of the Double-screw Processor or Extruder. *Plast. Polym.* **1975**, *43*, 93–98.
34. Nastaj, A.; Wilczyński, K. Scaling-Up for the Counter-Rotating Twin Screw Extrusion of Polymers. *Polymers* **2024**, *16*, 2720. [CrossRef]
35. Klein, I.; Tadmor, Z. The simulation of the plasticating screw extrusion process with a computer programmed theoretical model. *Polym. Eng. Sci.* **1969**, *9*, 11–21. [CrossRef]
36. Acur, E.E.; Vlachopoulos, J. Numerical simulation of a single-screw plasticating extruder. *Polym. Eng. Sci.* **1982**, *22*, 1084–1094. [CrossRef]
37. Amellal, K.; Lafleur, P.G.; Arpin, B. A Computer Model for the Simulation of Conventional and Barrier Screws. *Polym.-Plast. Technol. Eng.* **1991**, *30*, 655–664. [CrossRef]
38. Macgregor, A.; Vlachopoulos, J.; Vlcek, J. Computer Simulation of Conventional and Barrier Screw Extruders. *J. Reinf. Plast. Compos.* **1997**, *16*, 1270–1280. [CrossRef]
39. Aigner, M.; Köpplmayr, T.; Kneidinger, C.; Miethlinger, J. A network-analysis-based comparative study of the throughput behavior of polymer melts in barrier screw geometries. *AIP Conf. Proc.* **2014**, *1593*, 606–610.
40. Stueker, D.; Schoeppner, V. Simplified numerical calculation of the isothermal, three-dimensional, Non-Newtonian flow characteristics of single-screw melt-extruder. *AIP Conf. Proc.* **2023**, *2607*, 060008.
41. Hube, S.; Behr, M.; Elgeti, S.; Schön, M.; Sasse, J.; Hopmann, C. Numerical design of distributive mixing elements. *Finite Elem. Anal. Des.* **2022**, *204*, 103733. [CrossRef]
42. Marschik, C.; Roland, W. Predicting the pumping capability of single-screw extruders: A comparison of two- and three-dimensional modeling approaches. *AIP Conf. Proc.* **2023**, *2607*, 020002.

43. Ershov, S.V.; Trufanova, N.M. Numerical studies of the polymer melt flow in the extruder screw channel and the forming tool. *IOP Conf. Ser. Mater. Sci. Eng.* **2017**, *208*, 012018. [CrossRef]
44. Kadyirov, A.; Gataullin, R.; Karaeva, J. Numerical Simulation of Polymer Solutions in a Single-Screw Extruder. *Appl. Sci.* **2019**, *9*, 5423. [CrossRef]
45. Lim, K.H.; Hwang, W.R.; Kim, S.J. A finite-element technique for flows in the single screw extruder using a partial periodic unit. *Korea-Aust. Rheol. J.* **2019**, *31*, 59–67. [CrossRef]
46. Vachagina, E.K.; Kadyirov, A.I.; Karaeva, J.V. Simulation of Giesekus fluid flow in extruder using helical coordinate system. *IOP Conf. Ser. Mater. Sci. Eng.* **2020**, *733*, 012033. [CrossRef]
47. Herzog, D.; Roland, W.; Marschik, C.; Berger-Weber, G.R. Generalized predictions of the pumping characteristics and viscous dissipation of single-screw extruders including three-dimensional curvature effects. *Polym. Eng. Sci.* **2024**, *64*, 5566–5587. [CrossRef]
48. Janßen, M.; Schiffers, R. Predicting the rotation speed of mixing sleeves in single-screw extrusion by means of CFD-simulation. *AIP Conf. Proc.* **2023**, *2607*, 020003.
49. Schöppner, V.; Schadomsky, M.; Hopmann, C.; Lemke, F. Investigations of the mixing behaviour of pin-type rubber extruders. *AIP Conf. Proc.* **2016**, *1713*, 130003.
50. Kimura, K.; Nakayama, Y.; Kajiwara, T. Distributive mixing characteristics of a Dulmage-type screw for a single-screw extruder: Experimental and numerical evaluation. *Chem. Eng. J. Adv.* **2021**, *7*, 100137. [CrossRef]
51. Erb, T.; Celik, O.; Bonten, C. Three-dimensional characterization of dispersive mixing in single screw extruders. *AIP Conf. Proc.* **2016**, *1779*, 050001.
52. Frank, M.; Hollenhorst, V.; Schöppner, V. Investigation of the pressure-throughput behaviour of different faceted mixer geometries on an analytical and simulative basis. *AIP Conf. Proc.* **2023**, *2607*, 060010.
53. Wang, Z.; Pan, Y.; Liu, Y.; Huang, J.; Wang, N.; Hu, X. Investigations of the Elongational Deformation Induced by Pins in Pin-Barrel Cold-Feed Extruders. *Adv. Polym. Technol.* **2022**, *2022*, 3513804. [CrossRef]
54. Marschik, C.; Osswald, T.A.; Roland, W.; Albrecht, H.; Skrabala, O.; Miethlinger, J. Numerical analysis of mixing in block-head mixing screws. *Polym. Eng. Sci.* **2019**, *59*, E88–E104. [CrossRef]
55. Motzigemba, M.; Broecker, H.C.; Prüss, J.; Bothe, D.; Warnecke, H.J. Chapter 37—A contribution to simulation of mixing in screw extruders employing commercial CFD-software. In *10th European Conference on Mixing*; van den Akker, H.E.A., Derksen, J.J., Eds.; Elsevier Science: Amsterdam, The Netherlands, 2000; pp. 297–304.
56. Straka, K.; Praher, B.; Steinbichler, G. Analyzing melt homogeneity in a single screw plasticizing unit of an injection molding machine. *AIP Conf. Proc.* **2013**, *1558*, 94–97.
57. Alemaskin, K.; Manas-Zloczower, I.; Kaufman, M. Color mixing in the metering zone of a single screw extruder: Numerical simulations and experimental validation. *Polym. Eng. Sci.* **2005**, *45*, 1011–1020. [CrossRef]
58. Domingues, N.; Gaspar-Cunha, A.; Covas, J.A. Computational and Experimental Study of Mixing in a Single Screw Extruder. *AIP Conf. Proc.* **2007**, *907*, 867–872.
59. Frank, M.; Schöppner, V. Investigation of the homogenization performance of various faceted mixers and optimization with regard to mixing as well as pressure throughput behavior. *AIP Conf. Proc.* **2023**, *2884*, 090003.
60. Liu, L.; Meng, Z.; Zhang, Y.; Sun, Y. Simulation of High-Viscosity Generalized Newtonian Fluid Flows in the Mixing Section of a Screw Extruder Using the Lattice Boltzmann Model. *ACS Omega* **2023**, *8*, 47991–48018. [CrossRef]
61. Pandey, V.; Maia, J.M. Extension-dominated improved dispersive mixing in single-screw extrusion. Part 1: Computational and experimental validation. *J. Appl. Polym. Sci.* **2021**, *138*, 49716. [CrossRef]
62. Pandey, V.; Maia, J.M. Comparative computational analysis of dispersive mixing in extension-dominated mixers for single-screw extruders. *Polym. Eng. Sci.* **2020**, *60*, 2390–2402. [CrossRef]
63. Wang, W.; Manas-Zloczower, I. Temporal distributions: The basis for the development of mixing indexes for scale-up of polymer processing equipment. *Polym. Eng. Sci.* **2001**, *41*, 1068–1077. [CrossRef]
64. Schulz, L.; Vorjohann, F.; Janßen, M.; Schiffers, R. Evaluating distributive mixing potential by mean distance of streamlines and a passive scalar. *AIP Conf. Proc.* **2023**, *2884*, 110004.
65. Kubik, P.; Zatloukal, M.; Vlcek, J.; Womer, T. Three-dimensional finite element method simulation study of fusion screw geometry. *Plast. Rubber Compos.* **2015**, *44*, 11–18. [CrossRef]
66. Moritzer, E.; Wittke, M.; Heiderich, G. Numerical simulation of residence time, shear rates and throughput in single screw extruders considering wall shear rates. *AIP Conf. Proc.* **2019**, *2065*, 030034.
67. Kim, S.J. Dimensionless analysis of three-dimensional residence time distribution in single-screw extrusion processes. *Korea-Aust. Rheol. J.* **2018**, *30*, 179–188. [CrossRef]
68. Olofsson, E.H.; Roland, M.; Spangenberg, J.; Jokil, N.H.; Hattel, J.H. A CFD model with free surface tracking: Predicting fill level and residence time in a starve-fed single-screw extruder. *Int. J. Adv. Manuf. Technol.* **2023**, *126*, 3579–3591. [CrossRef]

69. Mateboer, T.J.; Hummel, C.; van Dijk, D.J.; Buist, J. To quantify mixing quality in a single screw extruder simulation. In Proceedings of the 14th International Conference on CFD in 6 Oil & Gas, Metallurgical and Process Industries SINTEF, Trondheim, Norway, 12–14 October 2020.
70. Hopmann, C.; Schön, M.; Reul, M.M.; Facklam, M. A Method for the Validation of Simulated Mixing Characteristics of Two Dynamic Mixers in Single-Screw Extrusion. *Polymers* **2020**, *12*, 2234. [CrossRef]
71. Strutt, D.; Tzoganakis, C.; Duever, T.A. Mixing analysis of reactive polymer flow in a single-screw extruder channel. *Polym. Eng. Sci.* **2000**, *40*, 992–1003. [CrossRef]
72. Roy, S.; Lawal, A. Isothermal Pseudo-2D Analysis of Reactive Extrusion in Single-Screw Extruders. *J. Reinf. Plast. Compos.* **2004**, *23*, 685–706. [CrossRef]
73. Habla, F.; Obermeier, S.; Dietsche, L.; Kintzel, O.; Hinrichsen, O. CFD Analysis of the Frame Invariance of the Melt Temperature Rise in a Single-screw Extruder. *Int. Polym. Process.* **2013**, *28*, 463–469. [CrossRef]
74. Manohar, B.; Periasamy, C. Computational fluid dynamics simulation of single screw extruders in cable industries. *IJRET Int. J. Res. Eng. Technol.* **2016**, *5*, 5.
75. Casari, N.; Fadiga, E.; Pinelli, M.; Suman, A.; Ziviani, D. CFD Simulations of Single- and Twin-Screw Machines with OpenFOAM. *Designs* **2020**, *4*, 2. [CrossRef]
76. Roland, W.; Marschik, C.; Kommenda, M.; Haghofer, A.; Dorl, S.; Winkler, S. Predicting the Non-Linear Conveying Behavior in Single-Screw Extrusion: A Comparison of Various Data-Based Modeling Approaches used with CFD Simulations. *Int. Polym. Process.* **2021**, *36*, 529–544. [CrossRef]
77. Abdel-Ghany, W.E.; Ebeid, S.J.; Fikry, I. Mechanical design aspects of single screw extruders using finite element analysis. *Int. J. Eng. Tech. Res. (IJETR)* **2015**, *3*, 2454–4698.
78. Marschik, C.; Roland, W.; Miethlinger, J. A Network-Theory-Based Comparative Study of Melt-Conveying Models in Single-Screw Extrusion: A. Isothermal Flow. *Polymers* **2018**, *10*, 929. [CrossRef]
79. Stritzinger, U.; Roland, W.; Berger-Weber, G.; Steinbichler, G. Modeling melt conveying and power consumption of co-rotating twin-screw extruder kneading blocks: Part A. Data generation. *Polym. Eng. Sci.* **2022**, *62*, 3721–3745. [CrossRef]
80. Van Der Wal, D.; Goffart, D.; Klomp, E.; Hoogstraten, H.; Janssen, L. Three-dimensional flow modeling of a self-wiping corotating twin-screw extruder. Part II: The kneading section. *Polym. Eng. Sci.* **1996**, *36*, 912–924. [CrossRef]
81. Eitzlmayr, A.; Khinast, J. Co-rotating twin-screw extruders: Detailed analysis of conveying elements based on smoothed particle hydrodynamics. Part 2: Mixing. *Chem. Eng. Sci.* **2015**, *134*, 880–886. [CrossRef]
82. Eitzlmayr, A.; Matić, J.; Khinast, J. Analysis of Flow and Mixing in Screw Elements of Co-Rotating Twin-Screw Extruders via SPH. *AIChE J.* **2016**, *63*, 2451–2463. [CrossRef]
83. Rios, A.C.; Gramann, P.J.; Osswald, T.A. Comparative study of mixing in corotating twin screw extruders using computer simulation. *Adv. Polym. Technol.* **1998**, *17*, 107–113. [CrossRef]
84. Goffart, D.; Van Der Wal, D.; Klomp, E.; Hoogstraten, H.; Janssen, L.; Breysse, L.; Trolez, Y. Three-dimensional flow modeling of a self-wiping corotating twin-screw extruder. Part I: The transporting section. *Polym. Eng. Sci.* **1996**, *36*, 901–911. [CrossRef]
85. Hinz, J.; Helmig, J.; Möller, M.; Elgeti, S. Boundary-conforming finite element methods for twin-screw extruders using spline-based parameterization techniques. *Comput. Methods Appl. Mech. Eng.* **2020**, *361*, 112740. [CrossRef]
86. Helmig, J.; Behr, M.; Elgeti, S. Boundary-conforming finite element methods for twin-screw extruders: Unsteady-temperature-dependent-non-Newtonian simulations. *Comput. Fluids* **2019**, *190*, 322–336. [CrossRef]
87. Helmig, J.; Key, F.; Behr, M.; Elgeti, S. Combining boundary-conforming finite element meshes on moving domains using a sliding mesh approach. *Int. J. Numer. Methods Fluids* **2021**, *93*, 1053–1073. [CrossRef]
88. Ishikawa, T.; Kihara, S.I.; Funatsu, K. 3-D numerical simulations of nonisothermal flow in co-rotating twin screw extruders. *Polym. Eng. Sci.* **2000**, *40*, 357–364. [CrossRef]
89. Dong, T.; Wu, J. Simulation of non-Newtonian flows in a partially filled twin-screw extruder by smoothed particle hydrodynamics. *Polym. Eng. Sci.* **2022**, *62*, 802–814. [CrossRef]
90. Bauer, H.; Matić, J.; Khinast, J. Characteristic parameters and process maps for fully-filled twin-screw extruder elements. *Chem. Eng. Sci.* **2021**, *230*, 116202. [CrossRef]
91. Lewandowski, A.; Wilczyński, K.J.; Nastaj, A.; Wilczyński, K. A composite model for an intermeshing counter-rotating twin-screw extruder and its experimental verification. *Polym. Eng. Sci.* **2015**, *55*, 2838–2848. [CrossRef]
92. Prashanth, S.R.; Arumugam, S.K.; Gangradey, R.; Mukherjee, S.; Kasthurirengan, S.; Behera, U.; Pabbineedi, G.; Mugilan, M. CFD modelling and performance analysis of a twin screw hydrogen extruder. *Fusion Eng. Des.* **2019**, *138*, 151–158.
93. Zhang, Y.; Jiang, X.; Fan, H.; Li, X. Optimization and Numerical Simulation of Outlet of Twin Screw Extruder. *MATEC Web Conf.* **2018**, *153*, 05004. [CrossRef]
94. Ilinca, F.; Hétu, J.-F. Three-dimensional finite element solution of the flow in single and twin-screw extruders. *Int. Polym. Process.* **2010**, *25*, 275–286. [CrossRef]

95. Hétu, J.-F.; Ilinca, F. Immersed boundary finite elements for 3D flow simulations in twin-screw extruders. *Comput. Fluids* **2013**, *87*, 2–11. [CrossRef]
96. Malik, M.; Kalyon, D.; Golba, J. Simulation of co-rotating twin screw extrusion process subject to pressure-dependent wall slip at barrel and screw surfaces: 3D FEM analysis for combinations of forward-and reverse-conveying screw elements. *Int. Polym. Process.* **2014**, *29*, 51–62. [CrossRef]
97. Valette, R.; Vergnes, B.; Coupez, T. Multiscale simulation of mixing processes using 3D-parallel, fluid-structure interaction techniques. *Int. J. Mater. Form.* **2008**, *1*, 1131–1134. [CrossRef]
98. Avalosse, T.; Rubin, Y.; Fondin, L. Non-isothermal modeling of co-rotating and contra-rotating twin screw extruders. *J. Reinf. Plast. Compos.* **2002**, *21*, 419–429. [CrossRef]
99. Alsteens, B.; Legat, V.; Avalosse, T. Parametric study of the mixing efficiency in a kneading block section of a twin-screw extruder. *Int. Polym. Process.* **2004**, *19*, 207–217. [CrossRef]
100. Xu, B.; Liu, Y.; He, L.; Chen, J.; Turng, L.S. Numerical study of mixing dynamics inside the novel elements of a corotating nontwin screw extruder. *Adv. Polym. Technol.* **2018**, *37*, 2478–2496. [CrossRef]
101. Bauer, H.; Matić, J.; Evans, R.C.; Gryczke, A.; Ketterhagen, W.; Sinha, K.; Khinast, J. Determining local residence time distributions in twin-screw extruder elements via smoothed particle hydrodynamics. *Chem. Eng. Sci.* **2022**, *247*, 117029. [CrossRef]
102. Valette, R.; Coupez, T.; David, C.; Vergnes, B. A Direct 3D Numerical Simulation Code for Extrusion and Mixing Processes. *Int. Polym. Process.* **2009**, *24*, 141–147. [CrossRef]
103. Robinson, M.; Cleary, P.W. Effect of geometry and fill level on the transport and mixing behaviour of a co-rotating twin screw extruder. *Comput. Part. Mech.* **2019**, *6*, 227–247. [CrossRef]
104. Oldemeier, J.P.; Schöppner, V. Analysis of the Dispersive and Distributive Mixing Effect of Screw Elements on the Co-Rotating Twin-Screw Extruder with Particle Tracking. *Polymers* **2024**, *16*, 2952. [CrossRef] [PubMed]
105. Kwag, D.S.; Lyu, M.Y.; Kim, W.S. A 3D Numerical Study of Fluid Flow and Heat Transfer in a Single Screw Extruder. *Int. Polym. Process.* **2002**, *17*, 95–101. [CrossRef]
106. Sarhangi Fard, A.; Anderson, P.D. Simulation of distributive mixing inside mixing elements of co-rotating twin-screw extruders. *Comput. Fluids* **2013**, *87*, 79–91. [CrossRef]
107. Ahmed, I.; Poudyal, H.; Chandy, A.J. Fill Factor Effects in Highly-Viscous Non-Isothermal Rubber Mixing Simulations. *Int. Polym. Process.* **2019**, *34*, 182–194. [CrossRef]
108. Sun, D.; Zhu, X.; Gao, M. 3D Numerical Simulation of Reactive Extrusion Processes for Preparing PP/TiO_2 Nanocomposites in a Corotating Twin Screw Extruder. *Materials* **2019**, *12*, 671. [CrossRef] [PubMed]
109. Bertrand, F.; Thibault, F.; Delamare, L.; Tanguy, P.A. Adaptive finite element simulations of fluid flow in twin-screw extruders. *Comput. Chem. Eng.* **2003**, *27*, 491–500. [CrossRef]
110. Eitzlmayr, A.; Khinast, J. Co-rotating twin-screw extruders: Detailed analysis of conveying elements based on smoothed particle hydrodynamics. Part 1: Hydrodynamics. *Chem. Eng. Sci.* **2015**, *134*, 861–879. [CrossRef]
111. Martelli, F.G. *Twin Screw Extruders: A Basic Understanding*; Springer: Berlin/Heidelberg, Germany, 1983.
112. Nakayama, Y.; Takemitsu, H.; Kajiwara, T.; Kimura, K.; Takeuchi, T.; Tomiyama, H. Improving mixing characteristics with a pitched tip in kneading elements in twin-screw extrusion. *AIChE J.* **2018**, *64*, 1424–1434. [CrossRef]